DISCRETE WALL JETS
IN QUIESCENT AIR

by J. D. McLean and H. J. Herring

1. Report No. NASA CR-2388	2. Government Accession No.	3. Recipient's Catalog No.
4. Title and Subtitle DISCRETE WALL JETS IN QUIESCENT AIR		5. Report Date MAY 1974
		6. Performing Organization Code
7. Author(s) J. D. McLean and H. J. Herring		8. Performing Organization Report No. None
9. Performing Organization Name and Address Princeton University James Forrestal Campus Princeton, New Jersey 08540		10. Work Unit No.
		11. Contract or Grant No. NGL 31-001-074
12. Sponsoring Agency Name and Address National Aeronautics and Space Administration Washington, D.C. 20546		13. Type of Report and Period Covered Contractor Report
		14. Sponsoring Agency Code

15. Supplementary Notes
Final Report. Project Manager, Seymour Lieblein, V/STOL and Noise Division, NASA Lewis Research Center, Cleveland, Ohio

16. Abstract

An experimental investigation was made of turbulent jet flows resulting from small, round nozzles discharging parallel to a smooth, flat wall in quiescent air. Nozzle axes were located 3.0 nozzle diameters above the wall surface. The case of a single nozzle and the case of a spanwise array of equally spaced nozzles were investigated. Several forms of approximate velocity profile similarity were noted, and the flow from the array of nozzles was seen to approach the form of a two-dimensional wall jet.

17. Key Words (Suggested by Author(s)) Discrete wall jets; Turbulent velocity profiles; Experimental jet mixing	18. Distribution Statement Unclassified - unlimited
	CAT. 12

19. Security Classif. (of this report) Unclassified	20. Security Classif. (of this page) Unclassified	21. No. of Pages 45	22. Price* $3.25

TABLE OF CONTENTS

A_j	area of jet nozzle
d	diameter of jet nozzle
$\bar{I}$	nondimensionalized impulse integral
p	pressure
$\bar{Q}$	nondimensionalized volume flux integral
S	spanwise nozzle spacing in multiple jet
U	velocity in the X (axial) direction
U_{max}	maximum velocity at a given X, Z coordinate
X	axial coordinate
Y	vertical coordinate
Y_j	height of nozzle axis above wall
Y_{max}	height above wall at which maximum value U_{max} occurs at a given X, Z coordinate
$Y_{1/2}$	height above wall $(> Y_{max})$ at which velocity is $1/2\ U_{max}$
Z	transverse coordinate
$Z_{1/2}$	transverse location at which $U_{max}(X,Z) = 1/2\ U_{max}(X,0)$

subscripts

j	at the nozzle exit
∞	outside the jet

INTRODUCTION

This report presents the results of an experimental study of wall jets of the type which result when discrete, axisymmetric jets, either singly or in arrays, are directed parallel to a smooth, flat wall. The term "discrete wall jet" is used to distinguish this type of flow from the more usual two-dimensional wall jet, which issues from a two-dimensional slot. Two discrete wall jet flows were investigated in the course of the experiments: A single jet; and a spanwise row of jets spaced at uniform intervals. This multiple jet arrangement, when viewed from a large distance compared to the spacing between the jets, is equivalent to a two-dimensional wall jet.

In all of the experiments, the jet nozzles were positioned so that their axes were 3.0 nozzle diameters above the surface of the wall. Thus the emerging jet behaved as a free jet until its width had grown sufficiently for it to interact with the wall. The vertical distance of 3.0 nozzle diameters was chosen because it is large enough for a free jet to become fully developed (i.e. effectively to "forget" the nozzle geometry) before it interacts with the wall. This gave the experiments a certain generality in that the jets which interacted with the wall were fully developed free jets whose characteristics were independent of the particular nozzle geometry. With this in mind, the single discrete wall jet can be considered to consist of three basic regions. The first region is the free jet region just mentioned (which would not exist if the nozzle were placed flush with the wall); the second region is where the form of the jet accommodates

itself to the presence of the wall, and in the third region the jet has assumed a far field form characteristic of a discrete wall jet and independent of the nozzle geometry or the height of the axis above the wall.

The multiple jet case presents a somewhat more complicated picture. In this case, depending on the relative magnitudes of the nozzle diameter, axis height, and lateral spacing, any of the three regions of the single discrete wall jet can be interupted by the merging of each jet with its neighbors. At whatever stage this merging process begins, however, the end product will be the same; if the jet is followed sufficiently far downstream, it will be seen to assume a form characteristic of a two-dimensional wall jet.

Free jets and two-dimensional wall jets have been subjects of a great deal of theoretical and experimental study. Much of this work has been reviewed by Abramovich [1] and Newman [2]. To the authors' knowledge, however, the case of a discrete wall jet issuing from an axisymmetric nozzle has not been studied directly. Prior to the present study, the only information available on discrete wall jet flow was from studies of closely related flows. Jets issuing from rectangular nozzles of various aspect ratios were studied experimentally by Sforza and Herbst [3], whose results seem to support the idea of a universal far field form for discrete wall jets. Patankar and Sridar [4] studied the behavior of the same type of jet (rectangular nozzle) on a convex wall. Knystautas [5] measured mean velocity profiles in a free jet produced by a closely spaced row of axisymmetric nozzles, showing that the flow became essentially two-dimensional

(at least in the mean) about 12 times the lateral jet spacing downstream of the nozzle exits. The assembly of nozzles was also placed adjacent to a convex wall, demonstrating that the Coanda effect was reduced in comparison with that of a two-dimensional jet.

One purpose of the present study is to investigate the quiescent air behavior of discrete wall jet configurations which could be of practical interest in applications of boundary layer control. One of the main advantages of discrete jets for boundary layer control will be in the structural simplicity of the installation in comparison with a two-dimensional jet slot. Full realization of this advantage dictates fairly large spacings between the jets in comparison with the nozzle diameter. Thus, the spacing chosen for the multiple jet portion of this study is large compared with those used by Knystautas.

EXPERIMENTAL APPARATUS AND PROCEDURE

The nozzle geometry which was used for both the single jet and multiple jet investigations is shown in Fig. 1. The nozzle is 0.085 inch in diameter and emerges from the side of a 0.375-inch O.D. thin wall stainless steel feed tube, with the axis of the nozzle perpendicular to the axis of the tube. The entire internal contour of the nozzle, including the flared inlet, was molded in epoxy, using steel molds inserted in the end of the tube. This manufacturing procedure produced nozzles of sufficient uniformity for the multiple jet experiments. The large area ratio between the feed tube and the nozzle was chosen to insure uniform flow at the nozzle exit. The velocity in the feed tube was low enough that friction losses could be ignored, and the jet stagnation pressure could be measured in the plenum chamber upstream.

The plenum chamber consisted of a length of 1 inch I.D. thick-walled pipe with holes drilled through one wall on 3-inch centers. Standard male flare fittings were soldered into these holes to be used as mounting points for the jet feed tubes. Eleven fittings were provided, so that eleven jet tubes could be accommodated for the multiple jet experiments. For the single jet experiments, only one jet tube was mounted, and the other ten mounting points were capped. When each jet tube was mounted, the alignment of the tube axis and the alignment, in yaw, of the nozzle axis were carefully adjusted before the flare fitting was tightened. Figure 2 shows the manifold (plenum chamber) mounted in the jig which was used for the single jet experiments and for jet tube alignment. One jet tube is shown in place with the handle used to apply leverage in making the yaw adjustment.

4

Yaw alignment was established by the probe in the background, which consisted of two open-ended tubes connected across a sensitive, low resistance mass flow meter. The tubes were positioned so as to straddle the desired jet axis. With the jet running, the jet tube was rotated until the mass flow meter indicated a null. In this application, the mass flow meter served as a sensitive null pressure indicator, indicating when the maximum velocity of the free jet was located halfway between the tubes of the probe. When acceptable alignment was attained, the nut on the flare fitting was tightened fully to lock the jet tube in place. The jet axes were aligned in this way, before the installation of the wall, for both the single jet and multiple jet experiments. It was found that the axes could be aligned to within 1/2 degree.

Figure 3 shows the flat wall installed for the single jet tests. The threaded legs allow the height of the table to be adjusted, thereby adjusting the distance between the jet axis and the wall surface. The multiple jet experiments were carried out on the flat top wall of a special wind tunnel constructed for boundary layer investigations. The tunnel entrance was blocked off so that there was no mean flow in the tunnel. The jet manifold was mounted outside the tunnel with the jet tubes projecting through holes in the test wall as shown in Fig. 4. In this case, the distance between the jet axes and the wall surface could be adjusted by moving the jet manifold assembly.

Air for the jets was supplied from large tanks at 2000 to 3000 psi. The high pressure was reduced through a regulator which maintained a stagnation pressure of 24.7 psia in the jet plenum chamber. A controllable

heater in the feedline was used to maintain the stagnation temperature equal to the room temperature, which averaged about 72°F. Assuming no losses between the plenum chamber and the nozzle exits, the nozzle exit velocity, U_j, was calculated to be 932 ft/sec, with a nozzle exit Mach number of 0.89. The structure of such a subsonic jet differs little from that of an incompressible one (see Snedeker and Donaldson [6]). The effects of compressibility are limited primarily to the region of the potential core immediately downstream of the nozzle exit. At distances large enough that the jet is fully developed, the jet is essentially incompressible, and the only effect of compressibility which remains is a possible shift in the apparent origin of the jet. This effect of compressibility is of no concern since, in these experiments, we are interested in the jet only after it has become fully developed.

The mean velocity measurements reported in later sections were made with small pitot tubes and static pressure tubes. The pitot tubes were made from stainless steel hypodermic tubing with .020-inch outside diameter and .010-inch inside diameter. The probe tips were carefully ground flat, perpendicular to the tube axes. The static pressure tubes were made from .032 inch outside diameter tubing with four .013 inch diameter holes drilled .25 inch from the sealed and rounded tip. Measurements made in a free jet by Bradshaw and Goodman [7] have shown that if a static pressure tube is sufficiently small compared to the dominant scales of the turbulence, the error in the probe reading due to turbulence will be small. The static tubes used in these experiments were small enough to satisfy this condition except when placed within a few tube diameters

of the wall. The measurements of Bradshaw and Goodman [7] were made on the axis of the free jet, where the turbulence fluctuation velocities are smaller than the mean velocity. Near the edge of a jet, the turbulence fluctuations can be larger than the mean velocity. In this region, where the mean velocity is low, errors in both the pitot pressure and the static pressure are likely to be significant. This effect results in some uncertainty in the integrals of mass and momentum flux. The seriousness of this uncertainty is discussed in the sections describing the experimental results.

The probe traversing mechanism which was used for both the single jet and multiple jet experiments was adapted from the compound rest of a lathe. A small D.C. motor was used to drive the screw feed very slowly during traverses, which were always made in the direction perpendicular to the wall. The X and Z coordinates of the probes were varied by moving the entire traversing mechanism. In the single jet case, the probes were used singly and were supported on struts from one side, as shown in Figs. 2 and 3. In the multiple jet case, the traversing mechanism was mounted outside the wind tunnel, and probes were mounted on a supporting rod which could be placed through any of a number of 3/8 in. diameter holes through the test wall. These holes were drilled in the test wall in a wide range of X and Z locations, and all of the holes except the one in use at any given time were covered on the flow side with thin plastic electrical tape. The tape was thin enough (.002 in.) that the edges of the tape strips were not judged to constitute significant roughness. For surveys of the multiple jet flows, the probe holder carried five pitot tubes simultaneously at the same X-Y station, but with each probe at a different Z (spanwise) location.

The five probes were equally spaced in such a way as to cover the spanwise distance between the plane of one jet centerline and a plane halfway to an adjacent jet centerline. Thus, the probes covered the region between a "peak" and a "trough" in the spanwise velocity profiles. For the static pressure measurements, only two probes were used; one at the "peak" and one at the "trough".

For convenience in data reduction, the data measured by the pitot and static pressure tubes were recorded on an X-Y plotter. The vertical location Y of the probe was measured by a Sanborn 7DC DT 2000 linear transformer, which was connected so as to drive one axis of the plotter. This measurement was calibrated at the beginning and end of each traverse against the micrometer graduations on the screw feed of the probe traverse mechanism. Pressures were measured by either a Pace CP51D-.1PSI transducer or a Statham 2732 P6-1.5D-120 transducer depending on the magnitude of the pressure being measured. The pressure transducer was calibrated at the end of each traverse against a Merriam 34FB2 micromanometer. Before data taking began, the overall response of the location and pressure measuring systems was found to be linear to within the accuracy of the plotter.

The pressure versus location plots which were produced in the course of the experiments were interpolated on an Oscar machine which recorded the data in the form of punched computer cards. A digital computer was then used to reduce the pressure data to velocity profiles, to plot the profiles, and to integrate the mass and momentum fluxes at each axial station. The mean velocity was calculated for all stations at which the pitot pressure was measured. To simplify the experiments, the static pressure was only

8

measured at a few representative stations, and in order to calculate the velocity at intermediate stations, the static pressure was interpolated linearly. This procedure was justified because the variations in static pressure were generally considerably smaller than the pitot pressure.

As an initial test of the instrumentation and of the quality of the flow produced by the nozzles, one of the nozzles was set up as a free jet. Velocity profiles were measured at two axial stations: $X = 4.40$ in. and $X = 8.80$ in. The profiles were found to be characteristic of a classical axisymmetric free jet, and the momentum flux at both stations agreed to within 1% with a one-dimensional compressible flow prediction for the nozzle. The maximum velocity U_{max} was measured at $X = 8.80$ in. for each of the eleven jets needed in the multiple jet array. These maximum velocities were found to be uniform to within ±3%.

RESULTS FOR THE SINGLE WALL JET

The general features of the single wall jet flow are illustrated in Fig. 5, which shows an isometric view of the measured mean velocity profiles. The maximum velocity is seen to decay rapidly with X, and the jet spreads rapidly in lateral extent. The vertical growth is slower than the lateral growth, providing evidence that the presence of the wall inhibits mixing in the vertical direction.

Figure 6 illustrates the terminology which is generally used in discussing wall jet velocity profiles. U_{max} is the maximum velocity, which occurs at a distance Y_{max} from the wall. In many analytical treatments, Y_{max} is used as the characteristic dimension of the flow near the wall. Farther from the wall, $Y_{1/2}$ is defined as the distance from the wall at which the velocity has decreased to one half of its maximum value. $Y_{1/2}$ (or in some cases $Y_{1/2} - Y_{max}$) is often used as the characteristic scale length of the outer flow. These definitions apply both on and off the plane of symmetry of the jet, and thus U_{max}, Y_{max} and $Y_{1/2}$ are functions of X and Z. $Z_{1/2}$ is defined as the spanwise distance from the plane of symmetry at which U_{max} has decreased to one half of its value on the plane of symmetry. $Z_{1/2}$ thus has meaning only in the single jet case and is a function only of X.

The velocity profiles on the plane of symmetry were found to assume an approximately similar form beginning with the profile measured at $X = 5.31$ in. Figure 7 shows these profiles plotted in the form U/U_{max} versus $Y/Y_{1/2}$. Only the profile at $X = 2.94$ in. is significantly different in

shape from the rest. The profiles off of the plane of symmetry were also found to approach an approximately similar form, but this similarity is less precise. Figure 8 shows that these profiles are roughly similar beginning with the measurements at $X = 8.31$ in. In Fig. 8, the profiles with a jagged appearance are those which were measured far from the plane of symmetry, where pressure differences were approaching the lower limit of resolution of the system. Increasing the sensitivity of the pressure measuring system in order to make measurements farther out in the fringe of the jet would not have yielded useful data because of the probability of errors due to turbulence in the readings of both probes. The spanwise profiles of the maximum velocity U_{max} at constant X, shown in Fig. 9, display a remarkable degree of similarity.

The vertical length scales in the plane of symmetry and the transverse length scale $Z_{1/2}$ are shown in Fig. 10. In the first interaction of the jet with the wall, Y_{max} decreases to less than one half of its initial value in the free jet region. Farther downstream, Y_{max} begins to increase slowly, as it must if the jet is to assume a similar or nearly self-preserving form. $Y_{1/2}$ and $Z_{1/2}$ both increase monotonically, their growth becoming nearly linear far downstream. The far field growth rate of $Y_{1/2}$ is smaller than the corresponding growth rate of an axisymmetric free jet, while the growth rate of $Z_{1/2}$ is faster than the free jet growth rate. As evidence that the jet is approaching a similar far field form, the ratios $Y_{max}/Y_{1/2}$ and $Z_{1/2}/Y_{1/2}$ appear to be approaching constant values far downstream. From dimensional analysis alone it is

reasonable to assume that the jet will take on a similar far field form in which the initial conditions, except for the momentum flux, are effectively "forgotten" by the jet.

Variations of the length scales out of the plane of symmetry are shown in Fig. 11. At stations corresponding with the initial interaction of the jet with the wall ($X = 2.94$ and $X = 5.31$), Y_{max} and $Y_{1/2}$ display sharp decreases away from the plane of symmetry. Farther downstream, $Y_{1/2}$ becomes nearly constant with Z. As $Y_{1/2}$ becomes constant with Z, the profile similarity shown in Fig. 8 becomes evident. (Note that in Fig. 8 the profiles are approximately similar starting with $X = 8.31$ in.). At the stations where $Y_{1/2}$ is nearly constant, $Y_{max}/Y_{1/2}$ has become roughly a single function of $Z/Z_{1/2}$ (Fig. 12), which is consistent with the idea of a similar far field form for the jet. The fact that $Y_{max}/Y_{1/2}$ increases somewhat with $Z/Z_{1/2}$ shows the profile similarity in the transverse direction (Fig. 8) is not precise. However, this transverse similarity is not necessary to the idea of a universal far field form.

The axial decay of U_{max} in the plane of symmetry is shown in Fig. 13. For comparison, the shaded area shows the region covered by the far field data from the rectangular nozzle flows of Sforza and Herbst [3]. From the slope of their data, Sforza and Herbst infer a velocity decay law: $U_{max} \propto X^{-1.15}$ Comparison with the present data indicates that they did not make measurements far enough downstream to see the true far field form of the jet. The present data seems to approach a universal

form closely only at the last two stations, and in this region an exponent of -1.23 is indicated for the decay law. In view of the similarity of velocity profiles and linear growth of the transverse and vertical length scales, an exponent less than minus one is consistent with the fact that jet momentum is being lost to skin friction.

Mean velocity profiles were measured in the center jet in an array of eleven jets. For the distances downstream at which measurements were made, it is reasonable to assume that the flow was representative of the flow from an infinite array of jets. An isometric view of the measured velocity profiles (Fig. 14) illustrates graphically how the growth of the jet is influenced by the merging with adjacent jets. It can be seen that the mean flow becomes uniform in the spanwise direction (two-dimensional) as the flow progresses downstream.

The teminology used in discussing the multiple jet profiles is the same as in the single jet case (Fig. 6), except that the jet spacing S becomes the pertinent dimension in the Z direction.

Velocity profiles in the plane of symmetry containing the axis of the center jet are shown in Fig. 15a and 15b. The profiles take considerably longer to become similar than do the corresponding profiles in the single jet case, Fig. 15b showing that the profiles are similar starting at X = 20.31 inches. Fig. 16, showing the profiles both on and off the plane of symmetry at several axial stations, illustrates more clearly the process taking place as the jets merge. By X = 8.31 inches, the profiles are similar, as they were in the single jet case.

At this early stage in the development of the flow, the jets are still essentially single jets. Farther downstream, the merging of the jets produces profiles which are definitely not similar (e.g. at X = 12.31 in. and 16.31 in.), and it is not until X = 24.31 in. that the

profiles become similar again. At X = 24.31 in., the mean velocity field
is not only similar, it is uniform in the Z direction (two-dimensional).
The progression from an essentially single jet flow to a spanwise-uniform
flow is clearly illustrated in the spanwise distribution of U_{max}, shown
in Fig. 17.

The vertical length scales of the profiles in the plane of symmetry
also illustrate this development (Fig. 18). For values of X up to
about 12 in., Y_{max} and $Y_{1/2}$ retain their single jet values. Farther
downstream, as the merging of the jets continues, Y_{max} and $Y_{1/2}$ grow
considerably faster than they do in the single jet, while the ratio
$Y_{max}/Y_{1/2}$ levels off at very nearly the far field value for the single
jet.

In the neighborhood of X = 20ᵣ25 in., where the flow has become
uniform in the spanwise direction, it might be expected that the flow
has assumed the structure of a classical planar wall jet. However, the
growth rate of $Y_{1/2}$ in this neighborhood is about 50% higher than the
growth rate of the fully developed planar wall jet. It is clear that,
although the mean flow profiles have assumed a two-dimensional form,
the turbulence structure has not yet relaxed to a fully developed two-
dimensional form. It is not until X = 30 in. or more that the growth
rate of $Y_{1/2}$ relaxes to a value characteristic of a planar wall jet.
Thus two-dimensionality, in terms of the mean flow profiles and the
growth rate, was reached about 10 nozzle spacings downstream of the
nozzle exits.

The spanwise distributions of the profile length scales are shown in Fig. 19, where it can be seen that Y_{max} and $Y_{1/2}$ become constant with Z by X = 24.31 in. At X = 5.31 in., $Y_{1/2}$ decreases away from the plane of symmetry, just as it did in the single jet case. But farther downstream, as adjacent jets merge, this trend is reversed, and $Y_{1/2}$ is seen to increase away from the plane of symmetry until it becomes uniform at X = 24.31 in. This is one of the more distinct changes in structure brought about by the merging of adjacent jets.

Figure 20 compares the maximum velocity decay of the multiple wall jet with that of the single wall jet. $U_{max}|_{Z=0}$ is the same in the near field for both cases until about X = 12 in., after which the multiple jet decays more slowly than the single jet. This slowing down of the decay rate is an expected result of the jet's assumption of a planar two-dimensional form; semi-infinite jets always decay more slowly than their finite counterparts. (Compare the planar free jet with its axisymmetric counterpart.) In the far field region, $U_{max}|_{Z=0}$ is seen to decay slightly faster than $X^{-1/2}$, which is consistent with the fact that momentum is being lost due to skin friction.

Interesting comparisons between the single wall jet and the multiple wall jet can be seen in the integrals across the jet of the mean velocity and the impulse. Fig. 21 shows the integral of the velocity (volume flux) normalized by a characteristic nozzle exit volume flux:

$$\overline{Q} = \frac{1}{\left(\frac{\rho_j}{\rho_\infty}\right)^{1/2} U_j A_j} \iint_{jet} u \, dy \, dz$$

Here the jet volume flux has been normalized by the nozzle exit volume flux of a hypothetical jet with $\rho_j = \rho_\infty$ but with the same diameter and momentum flux as the actual jet. $\bar{Q}$ defined in this way is a universal function of X/d (nearly independent of Reynolds number) for axisymmetric free jets. For the single wall jet, the integration covered the entire jet, while for the multiple jet the integration covered only the region which by symmetry can be considered to "belong" to a single nozzle ($-S/2 \leq Z \leq S/2$). Values for the single jet are seen to be almost identical to corresponding values for a free jet (adapted from the data of Hill [8]). This implies that the presence of the wall had very little effect on the total entrainment for $X/Y_j \lesssim 50$, or that the enhancement of the lateral spreading of the jet caused by the wall was sufficient to compensate for the reduction of the vertical spreading. At the last data point, $\bar{Q}$ begins to fall below the free jet line, and it must be assumed that eventually it would fall increasingly far below because of skin friction.

The entrainment rate for the multiple jet begins to fall below free jet values as soon as adjacent jets begin to merge, as shown by the fact that $\bar{Q}$ falls below the free jet line for all $X/Y_j \lesssim 20$. It is not possible to differentiate $\bar{Q}$ to obtain actual numerical entrainment rates because of scatter caused by uncertainties in the measurements of small velocities near the edge of the jet.

Shown in Fig. 22 are values of the jet impulse integral normalized by the nozzle exit impulse:

$$\overline{I} = \frac{1}{\rho_j U_j^2 A_j} \int\int_{jet} [\rho u^2 + (p-p_\infty)] \; dy \; dz$$

The decrease in $\overline{I}$ due to skin friction can be seen for both the single jet and the multiple jet. The single jet data do not go far enough downstream to show any discernable difference between the two types of jet in terms of $\overline{I}$, and the scatter does not allow differentiation to obtain skin friction coefficients.

SUMMARY

Two sets of velocity profile data are reported for jets in quiescent air. One is for the case of a single tangential wall jet and the other is for multiple tangential wall jets. The profile data exhibit strong lateral and longitudinal similarity in some regions of the jets. The wall jets spread more rapidly in the lateral direction and less rapidly in the normal direction then do free jets. Finally, far downstream the maximum jet velocity for both the single and multiple wall jets decays more rapidly than does the free jet.

REFERENCES

[1] Abramovich, G. N., (1963), <u>The Theory of Turbulent Jets</u>, M.I.T. Press.

[2] Newman, B. G., (1969), "The Prediction of Turbulent Jets and Wall Jets",
<u>Canadian Aeronautics and Space Journal</u>, Vol. 15, No. 8.

[3] Sforza, P. M. and Herbst, G., (1967), "A Study of Three Dimensional,
Incompressible Turbulent Wall Jets", Polytechnic Institute of
Brooklyn, Department of Aerospace Engineering and Applied Mechanics,
PIBAL Report No. 1022.

[4] Patankar, V. M. and Sridhar, K., (1971), "Three Dimensional Curved
Wall Jets", ASME Paper No. 71-WA/FE-2.

[5] Knystautas, R., (1964), "The Turbulent Jet from a Series of Holes in
Line", <u>Aeronautical Quarterly</u>, Vol. 15, pp. 1-28.

[6] Snedeker, R. S. and Donaldson, C. duP., (1964), "Experiments on Free
and Impinging Underexpanded Jets from a Convergent Nozzle",
Aeronautical Research Associates of Princeton, Inc., ARAP Report
No. 63.

[7] Bradshaw, P. and Goodman, D. G., (1968), "The Effect of Turbulence on
Static-Pressure Tubes", Gt. Britain, A.R.C., R&M No. 3527.

[8] Hill, B. J., (1972), "Measurement of Local Entrainment Rate in the
Initial Region of Axisymmetric Turbulent Air Jets", <u>J. Fluid
Mech.</u>, Vol. 51, part 4, pp. 773-779.

EPOXY FAIRING

NOZZLE EXIT

STAINLESS STEEL TUBE WALL
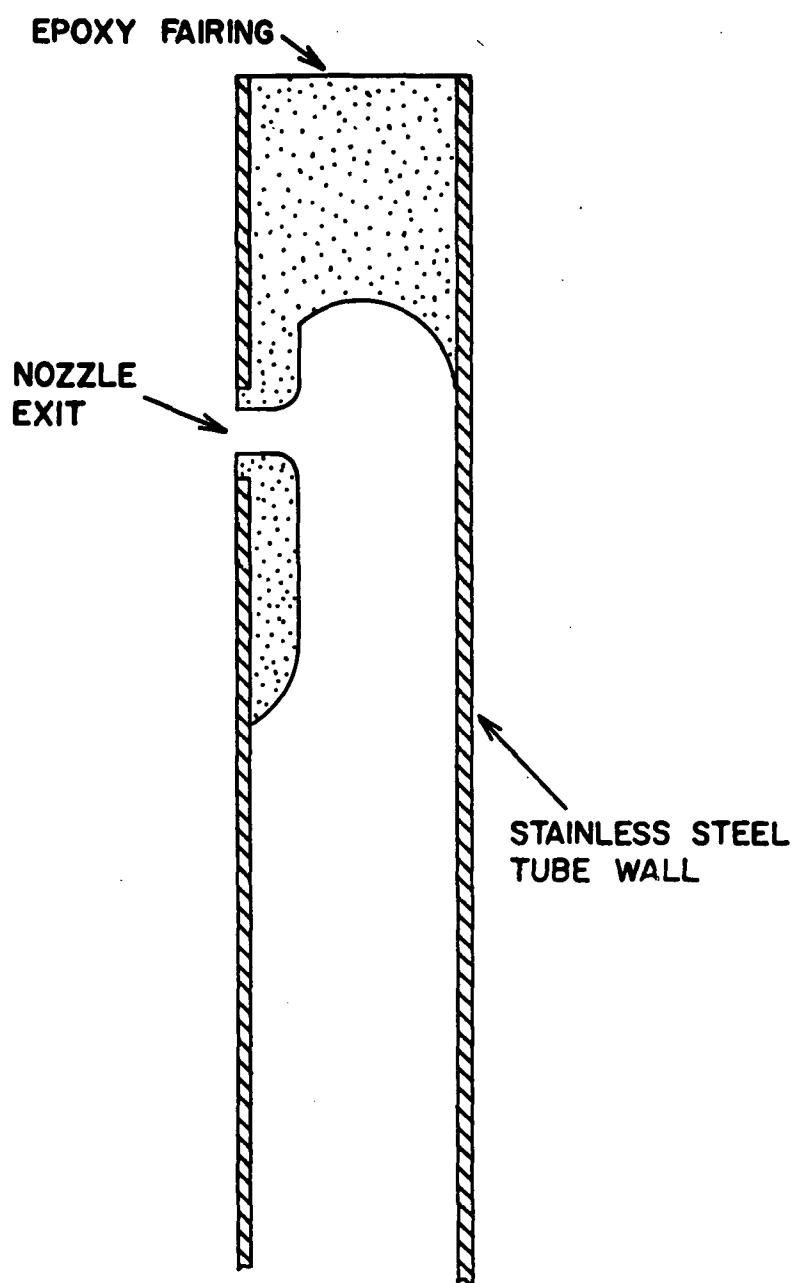
Figure 1. Cross-section of the jet nozzle.

ALIGNMENT PROBE

TRAVERSE MECHANISM

PITOT TUBE

MASS FLOW METER
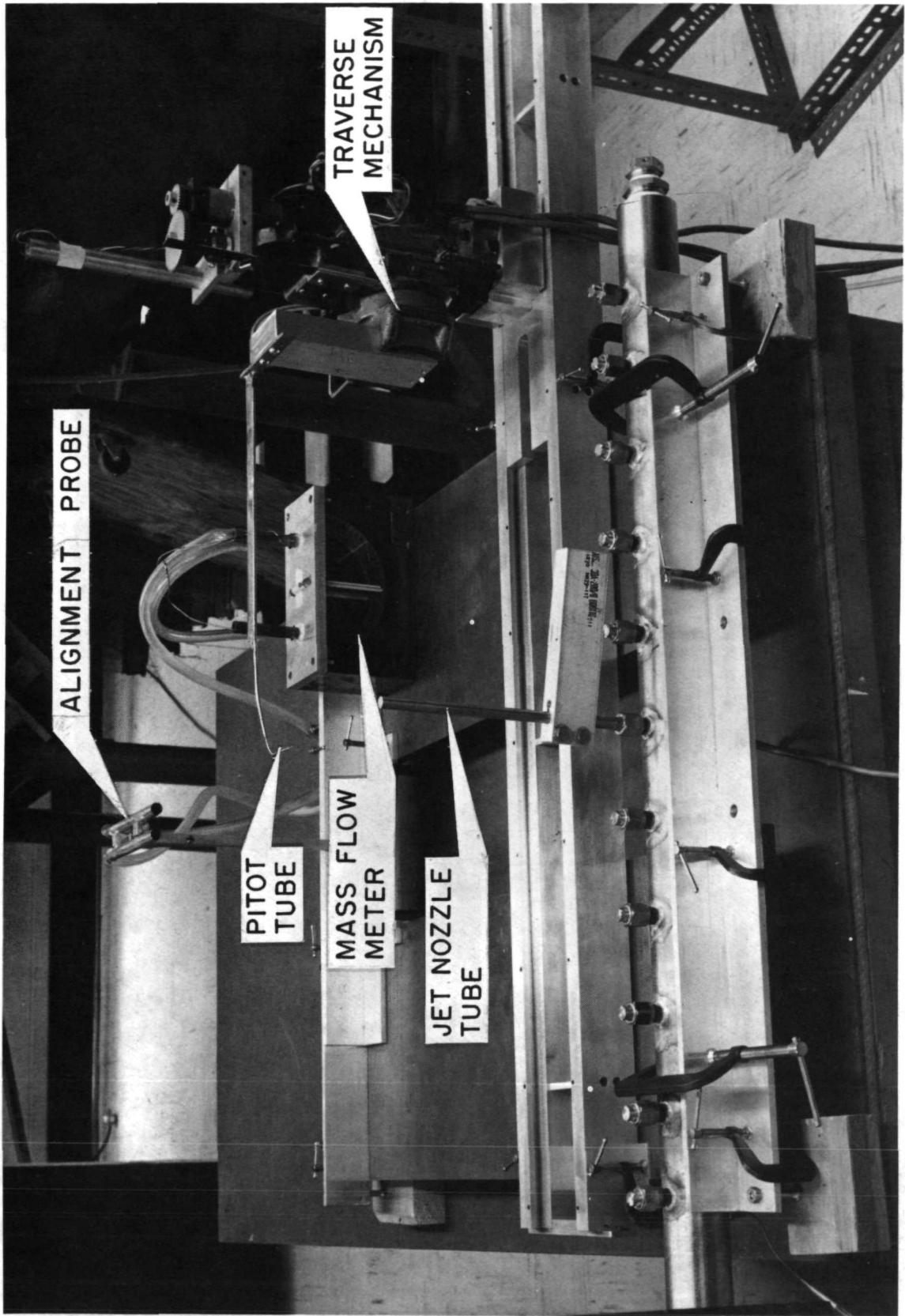
JET NOZZLE TUBE

Figure 2. The test rig with a single jet nozzle in place.

21

ALIGNMENT PROBE

TEST WALL

PITOT TUBE

JET NOZZLE
TUBE
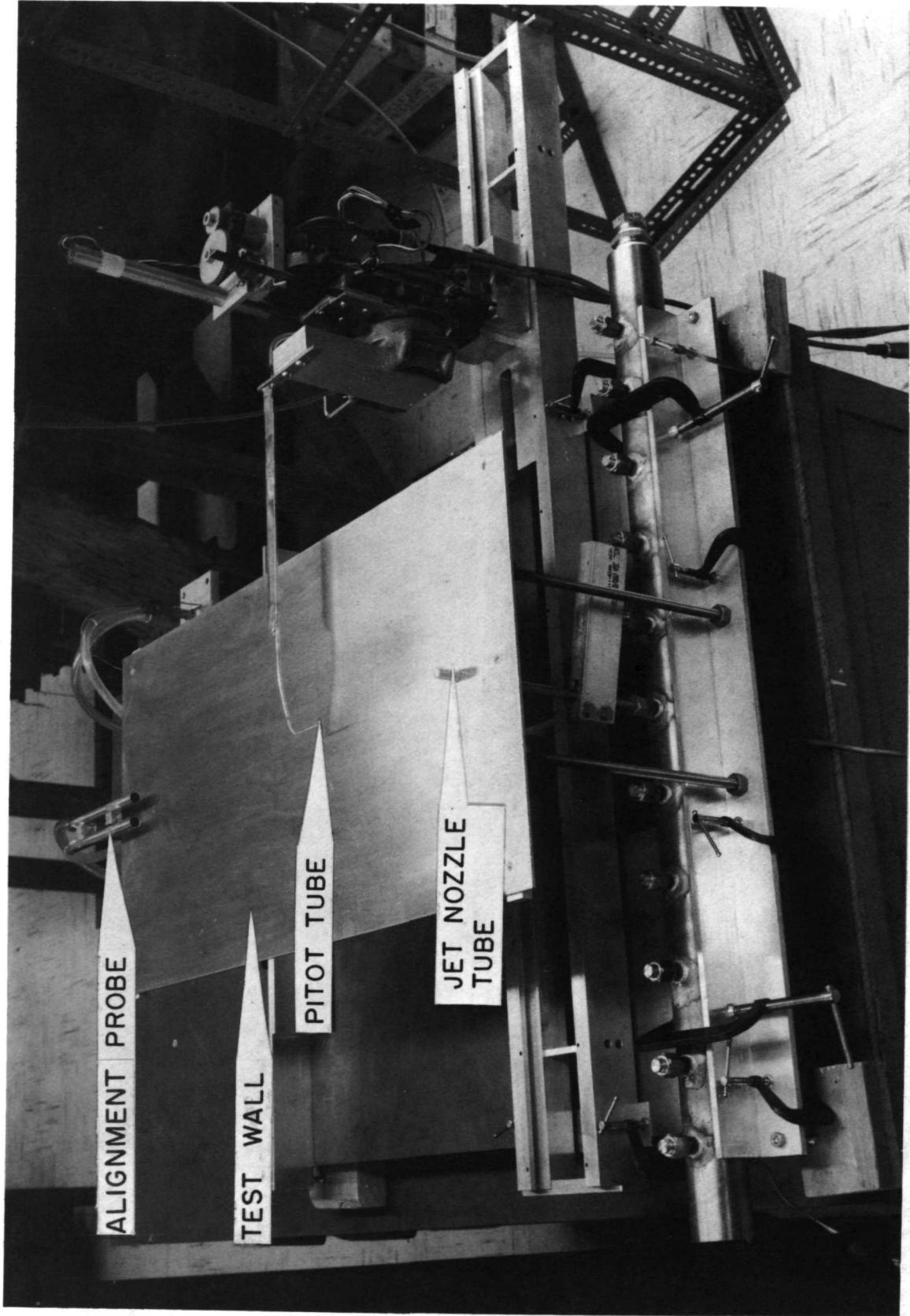
Figure 3. The test rig with the test wall and a single nozzle in place.
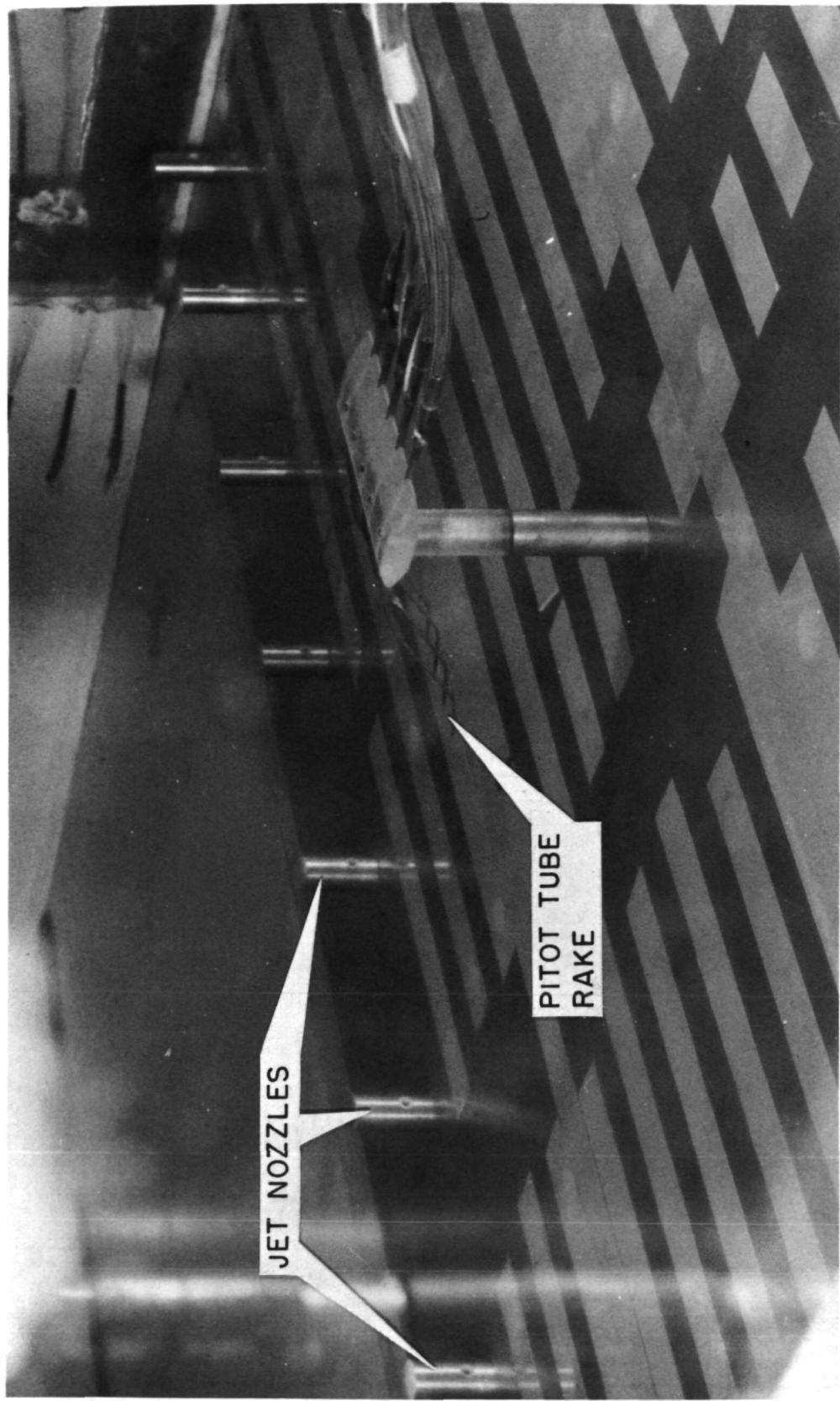
Figure 4. View of the wind tunnel test wall with multiple nozzles and the pitot tube rake in place.
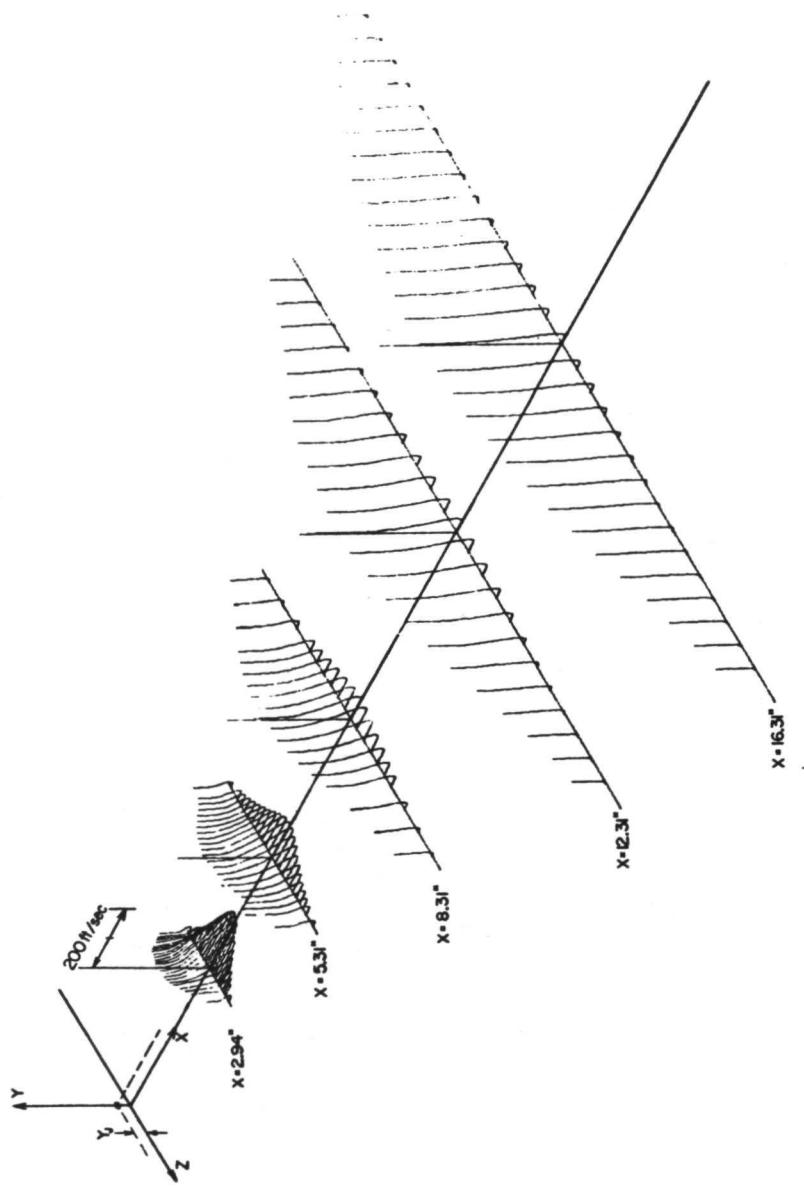
Figure 5. Isometric view of mean velocity profiles in the single discrete wall jet.

24
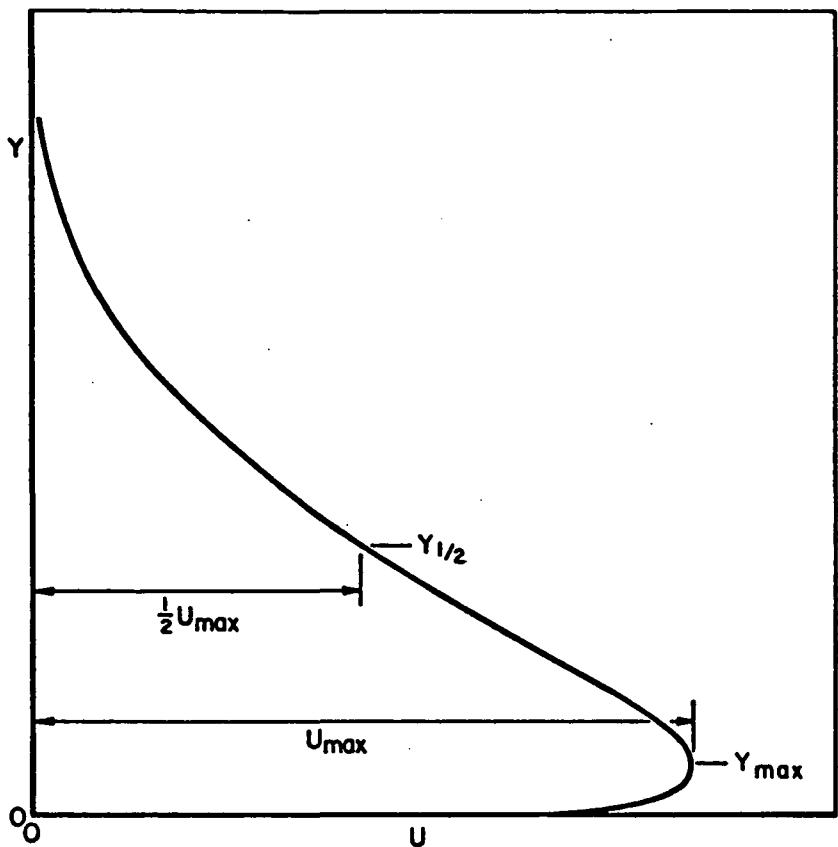
Figure 6a.   Schematic velocity profile illustrating
             profile terminology.
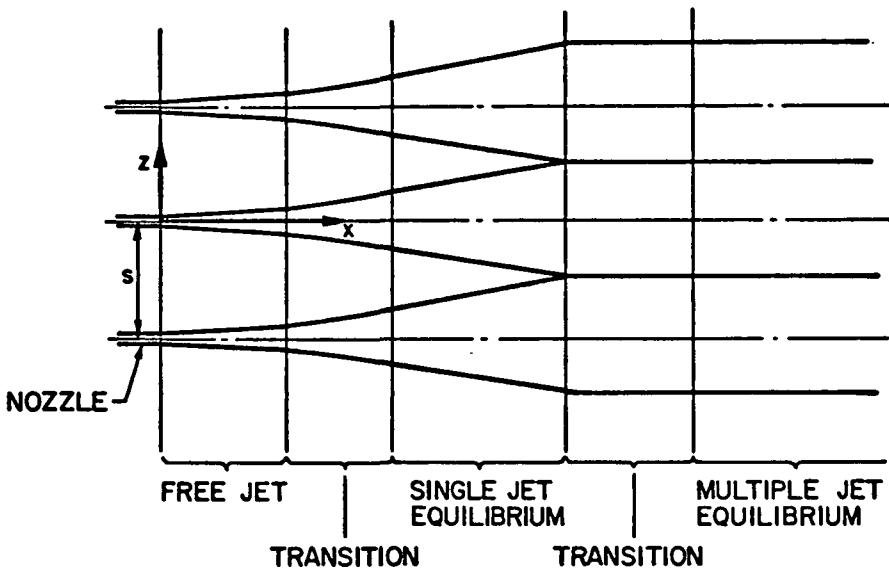
Figure 6b.   Illustration of various regions in the
             longitudinal development of the jets.

25
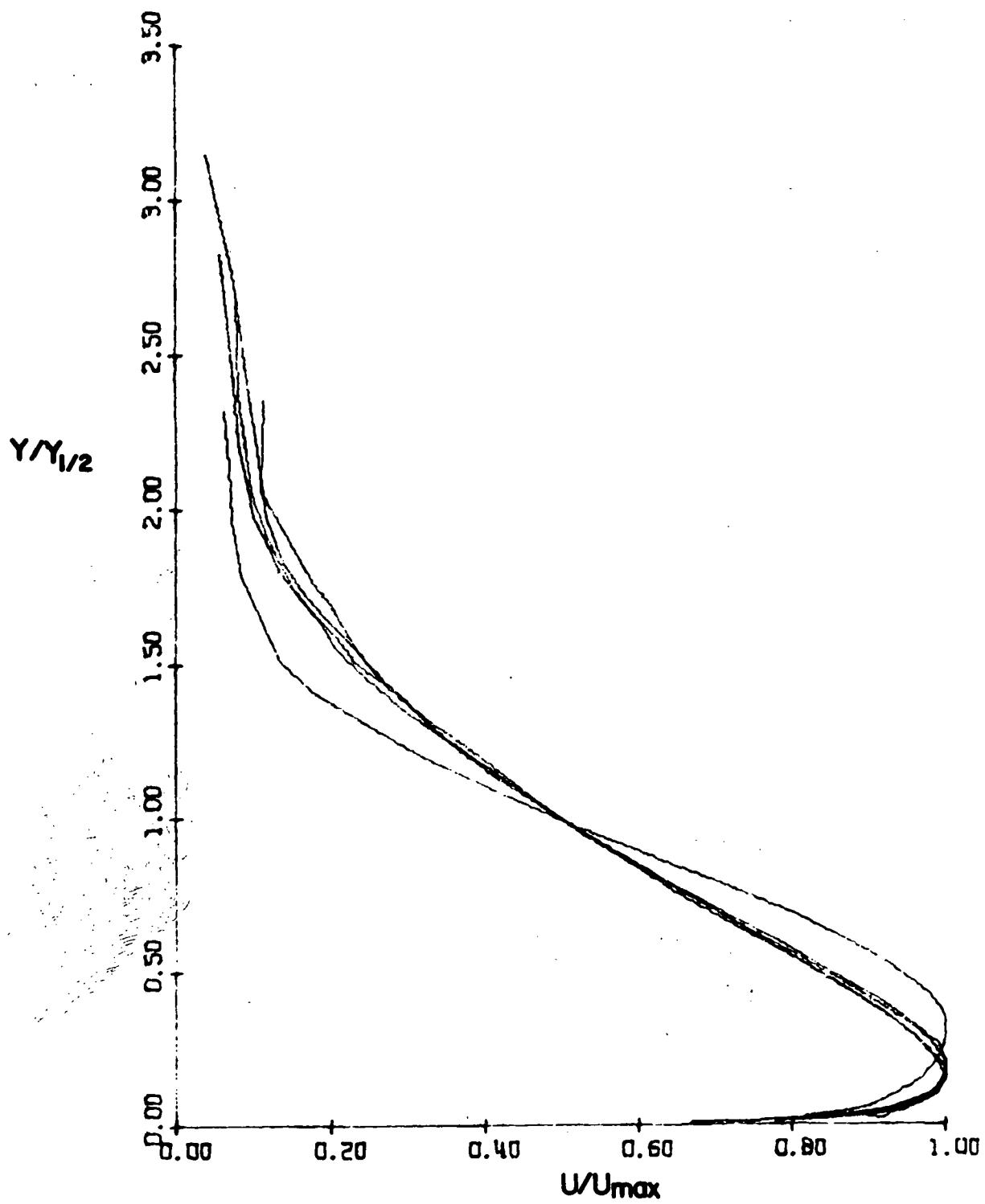
Figure 7. Single wall jet profiles along the nozzle
centerline (Z = 0).

26
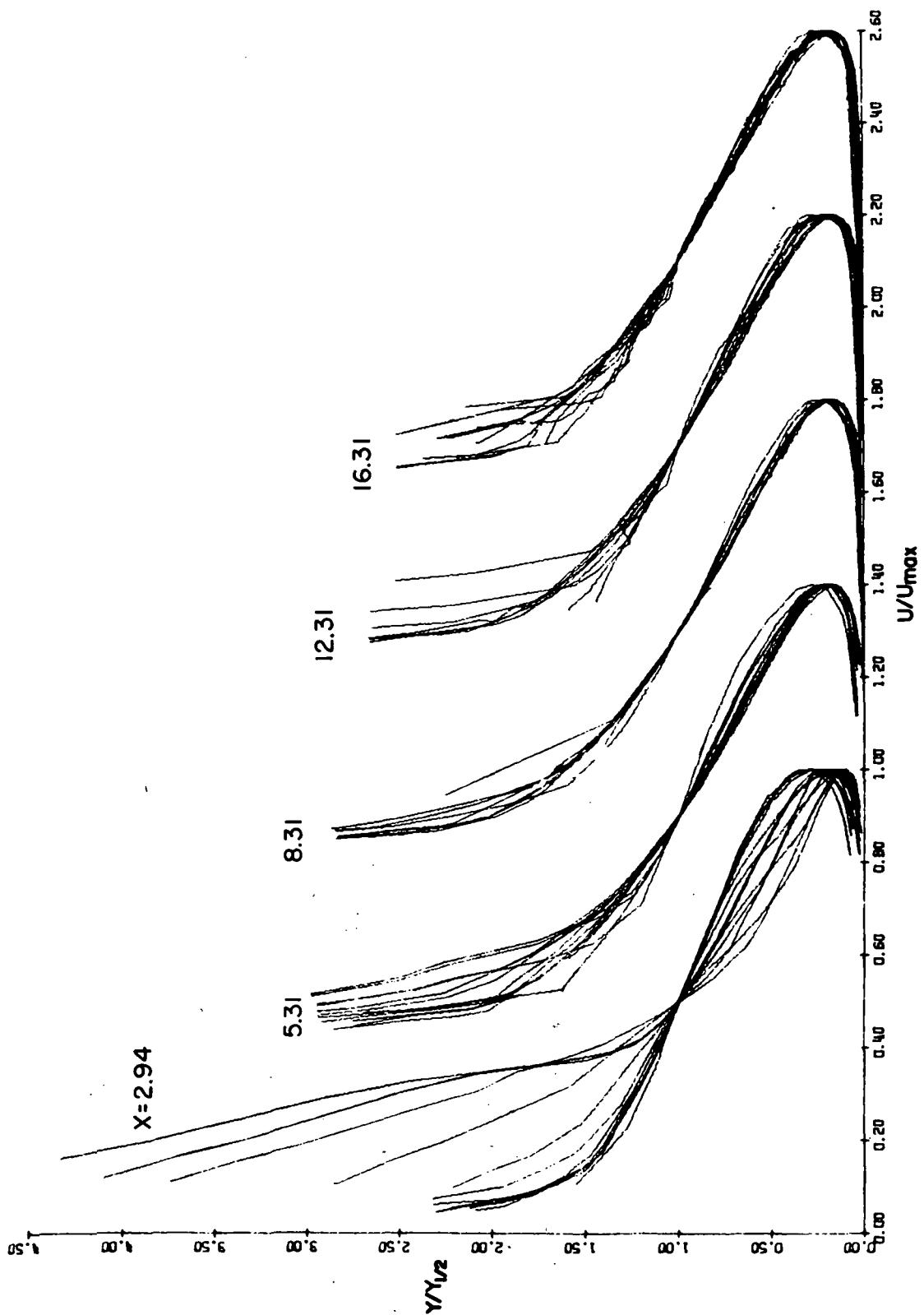
Figure 8. Single wall jet velocity profiles, including profiles off the centerline.

27
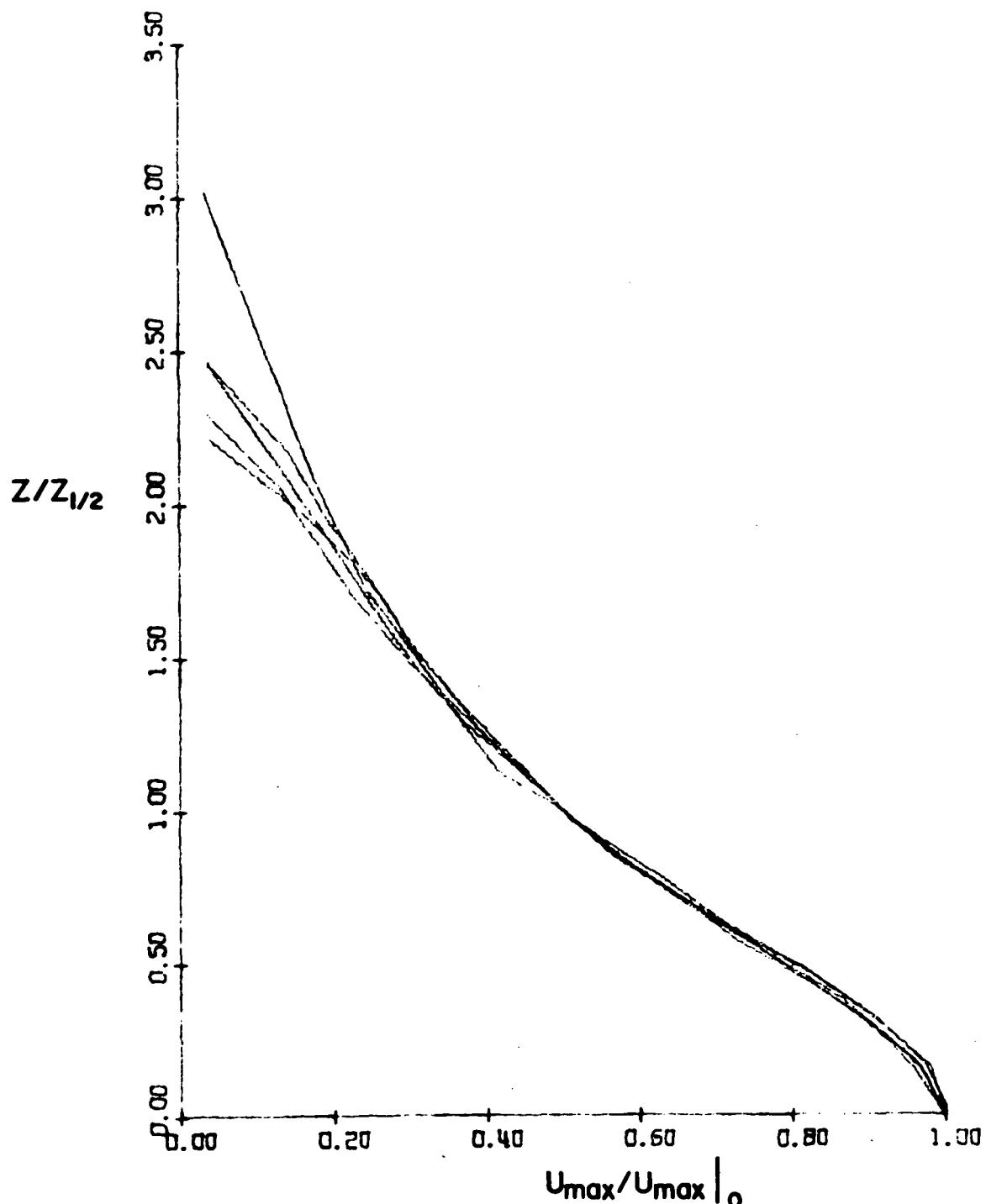
Figure 9. Transverse profiles of the maximum velocity in the single wall jet.
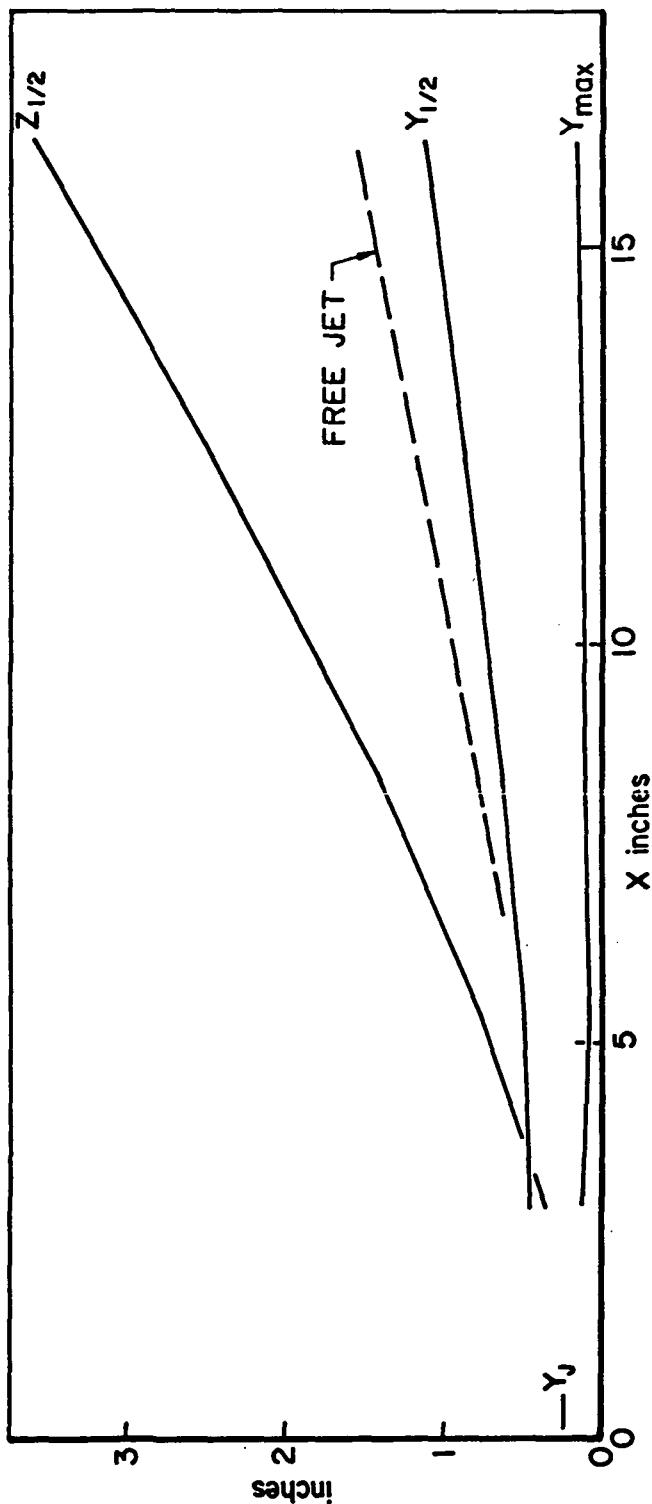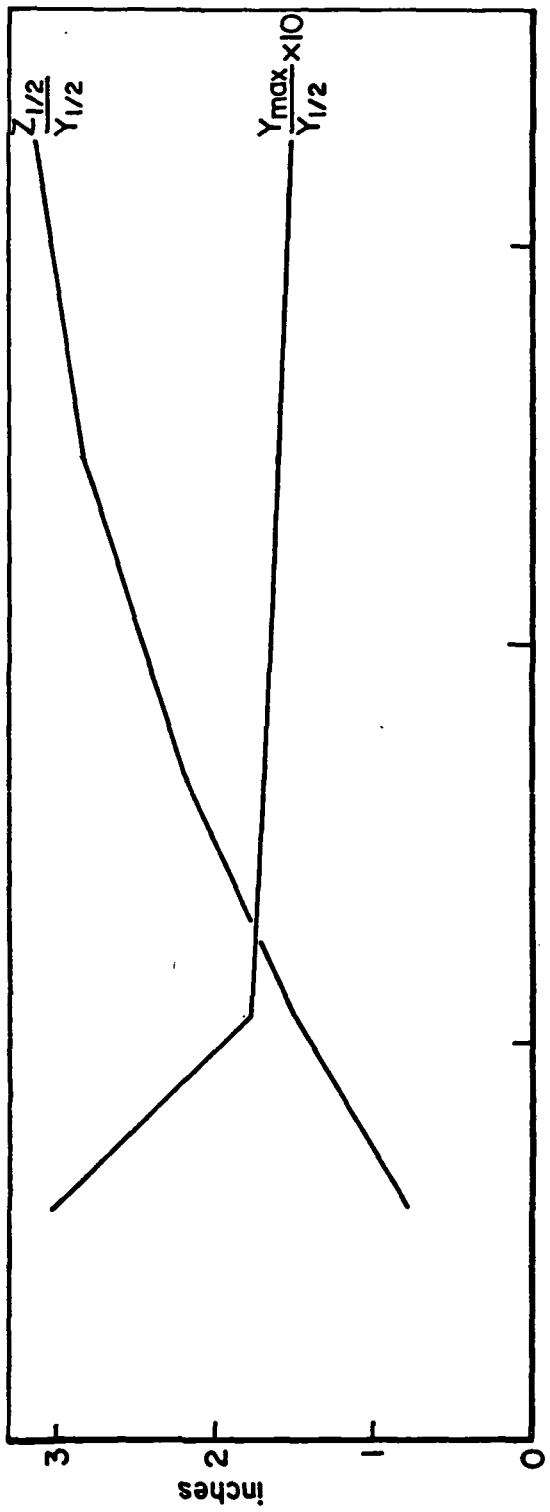
Figure 10. Axial variation of the primary length scales of the single wall jet.
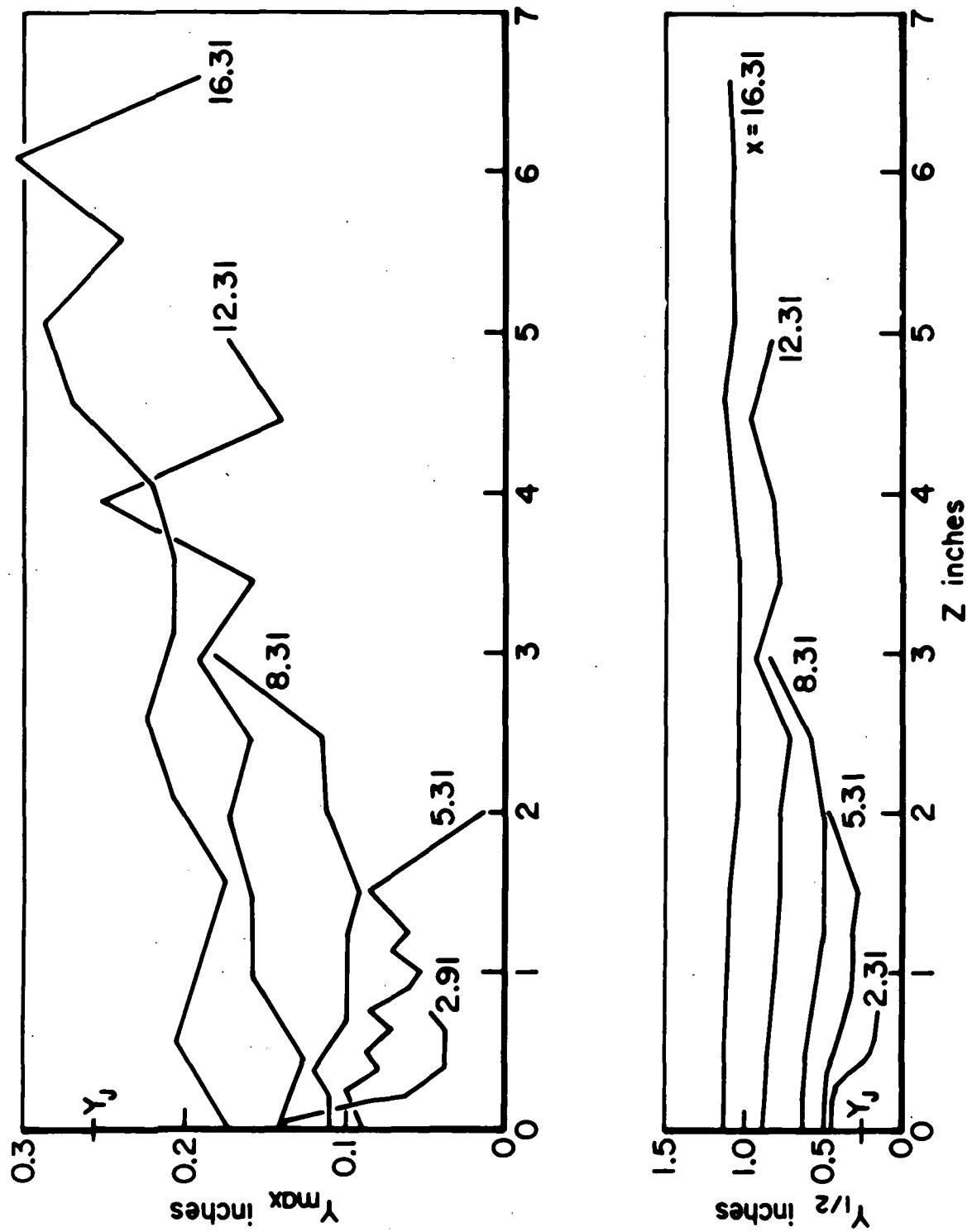
Figure 11. Transverse varation of length scales in the single wall jet.

30
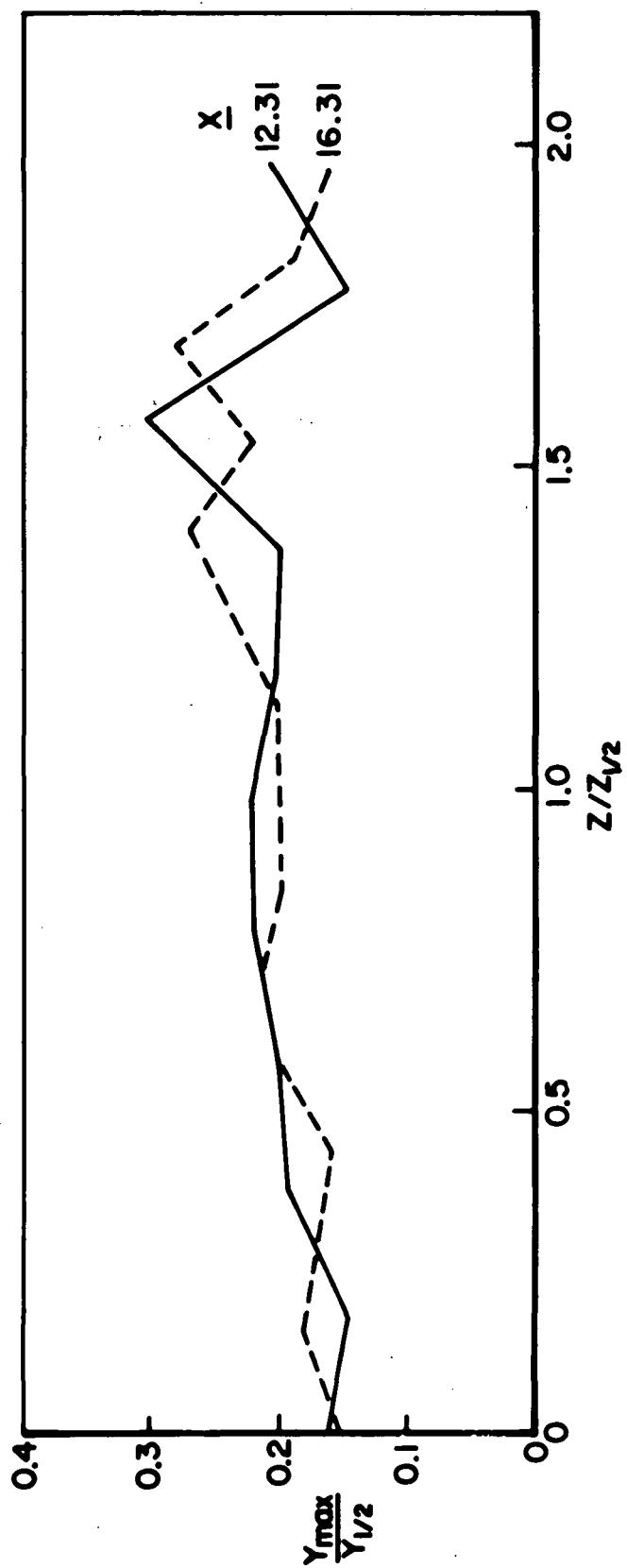
Figure 12. Transverse distribution of the ratio $Y_{max}/Y_{1/2}$ in the downstream region of the single wall jet.
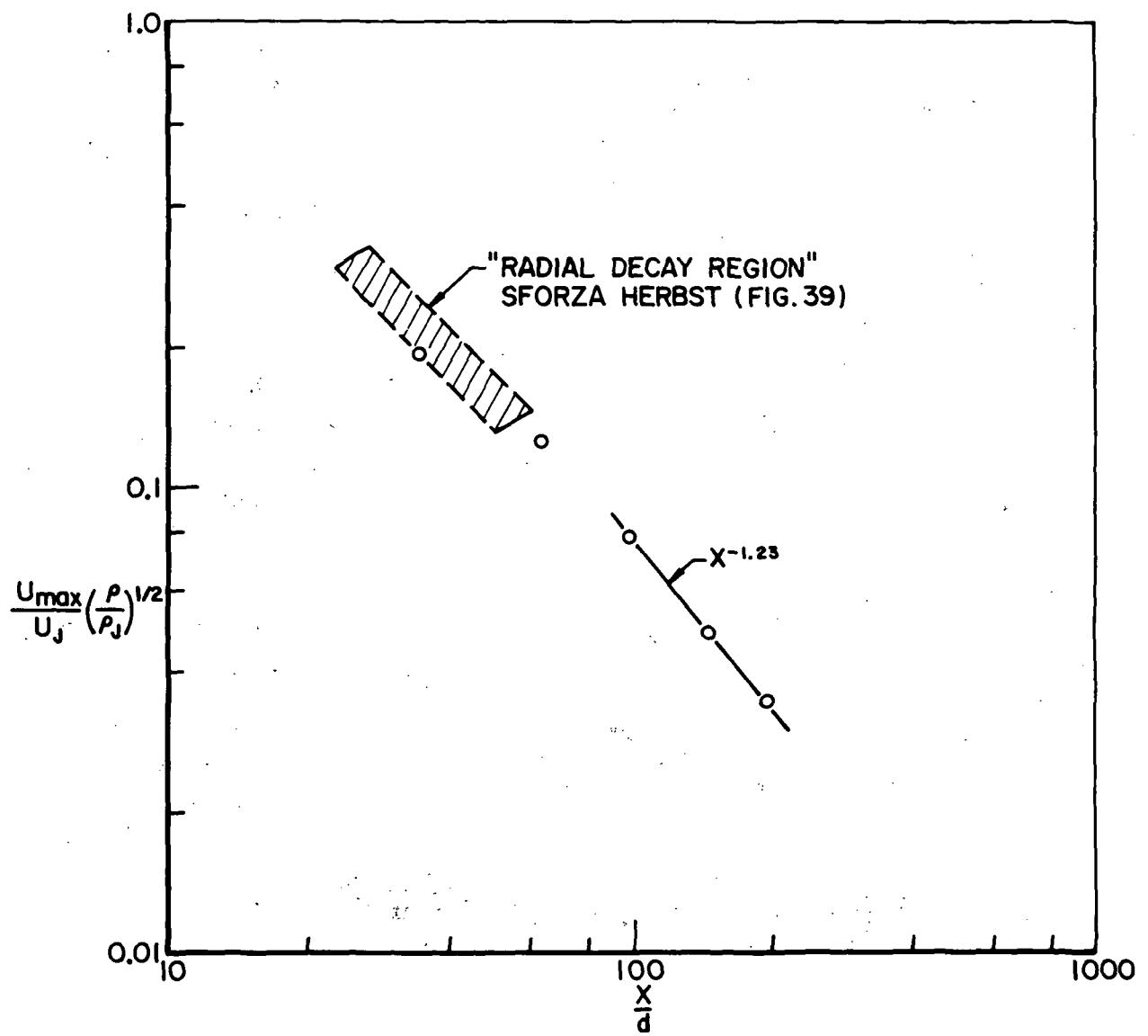
Figure 13. Axial decay of the centerline maximum velocity in the single wall jet.
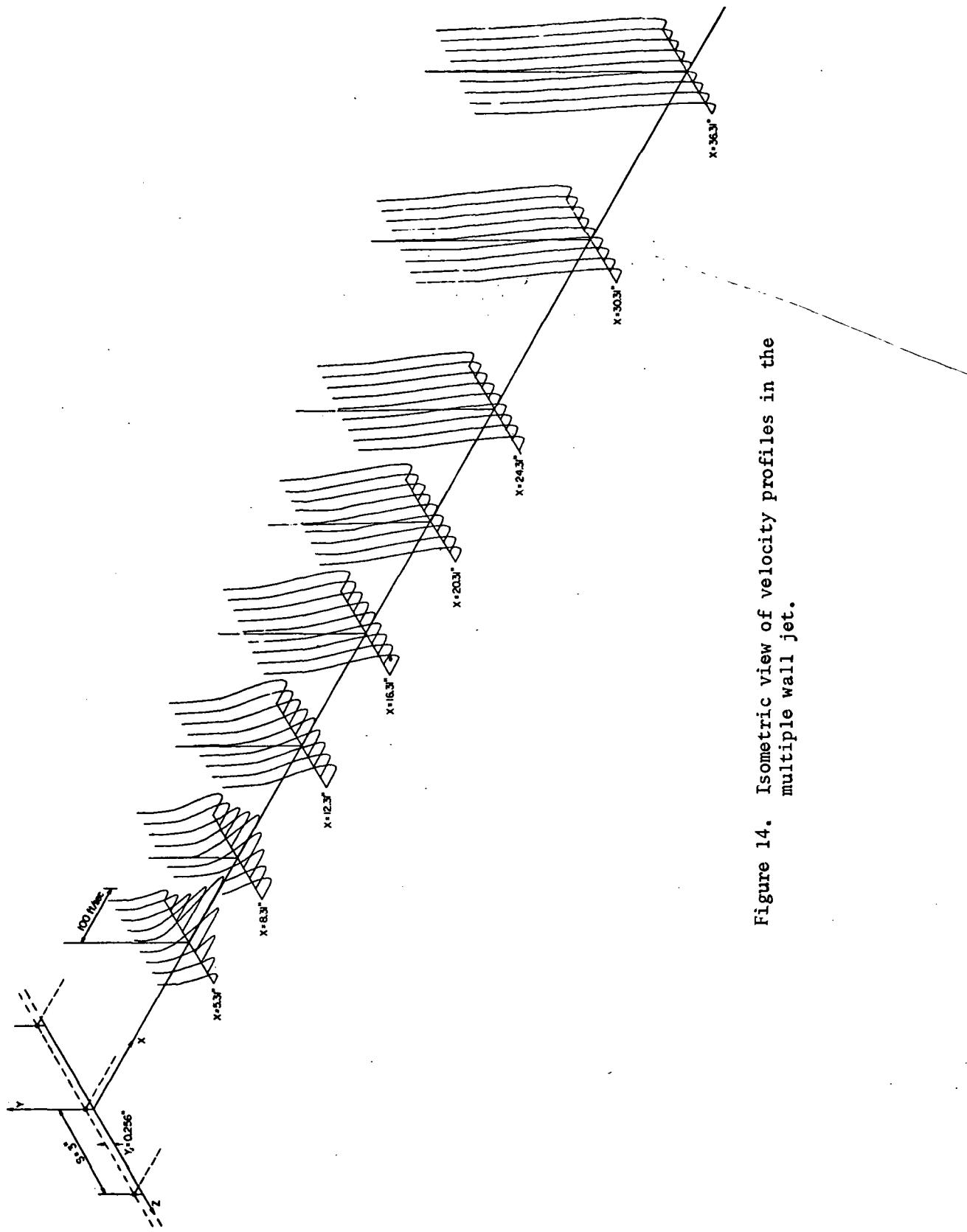
Figure 14. Isometric view of velocity profiles in the multiple wall jet.

33
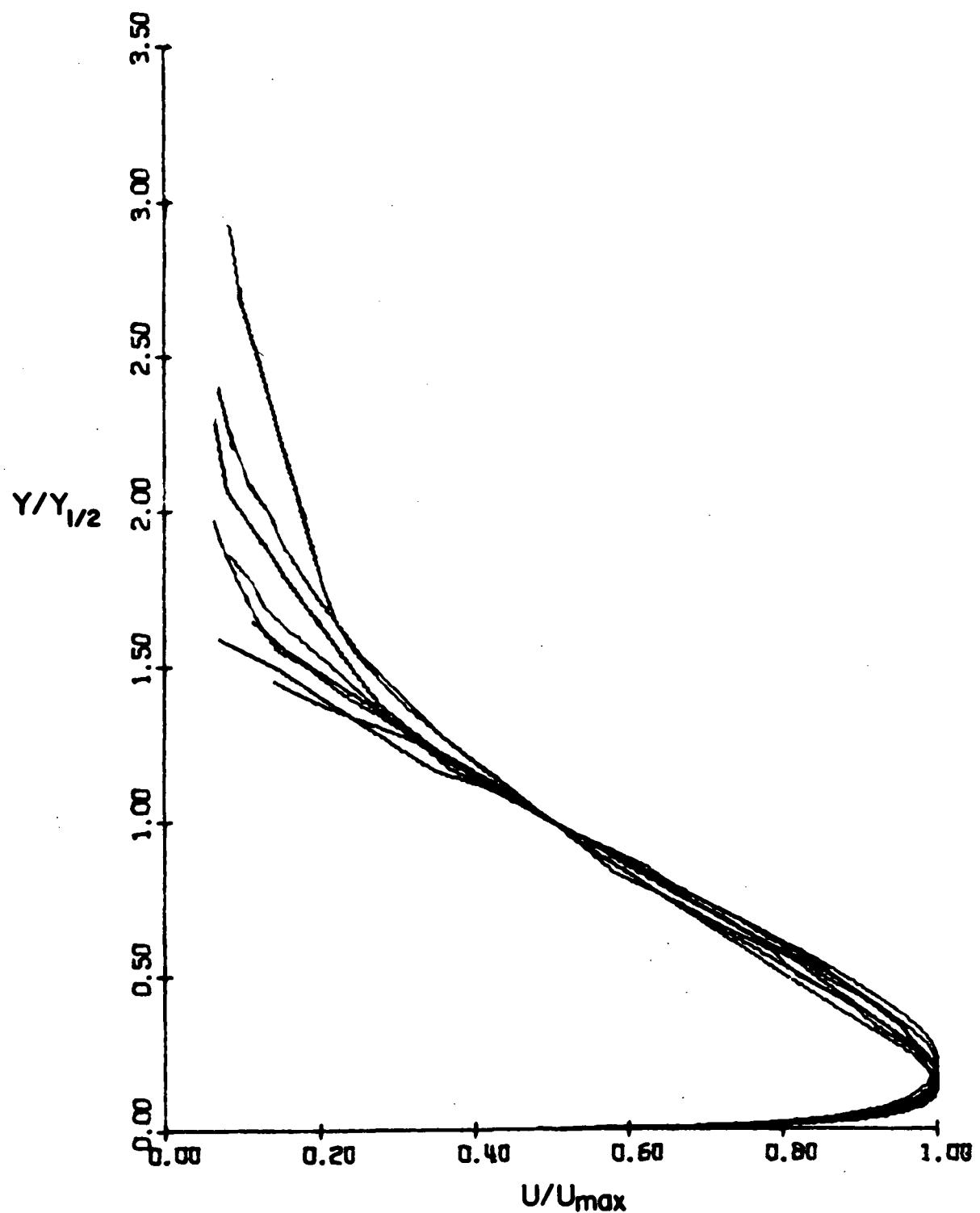
Figure 15a. Multiple wall jet velocity profiles along a
nozzle centerline for all X stations.

34
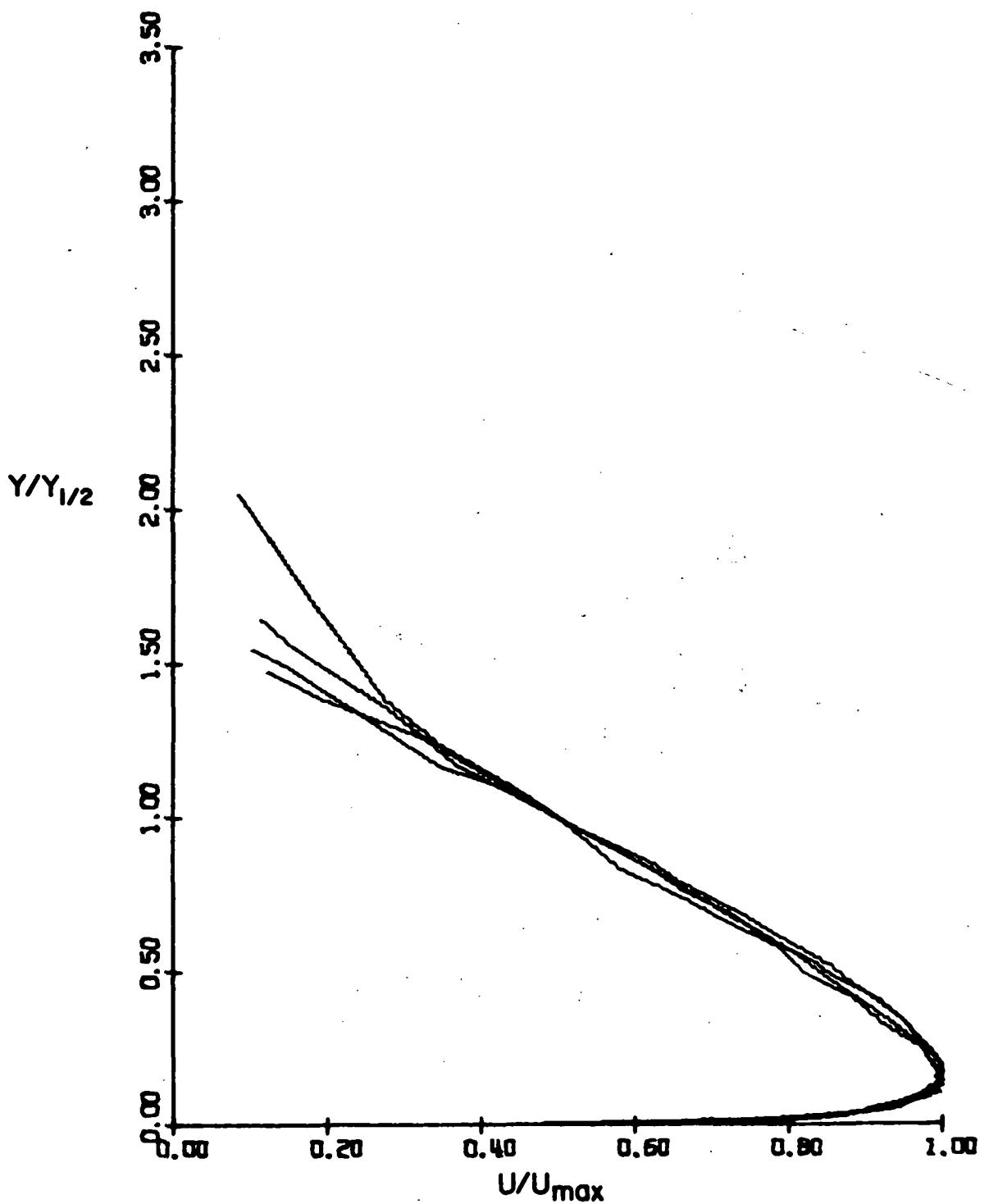
Figure 15b. Velocity profiles along a nozzle centerline
in downstream region of the multiple wall jet.
Profiles are shown for X = 20.31", 24.31",
30.31", and 36.31".

35
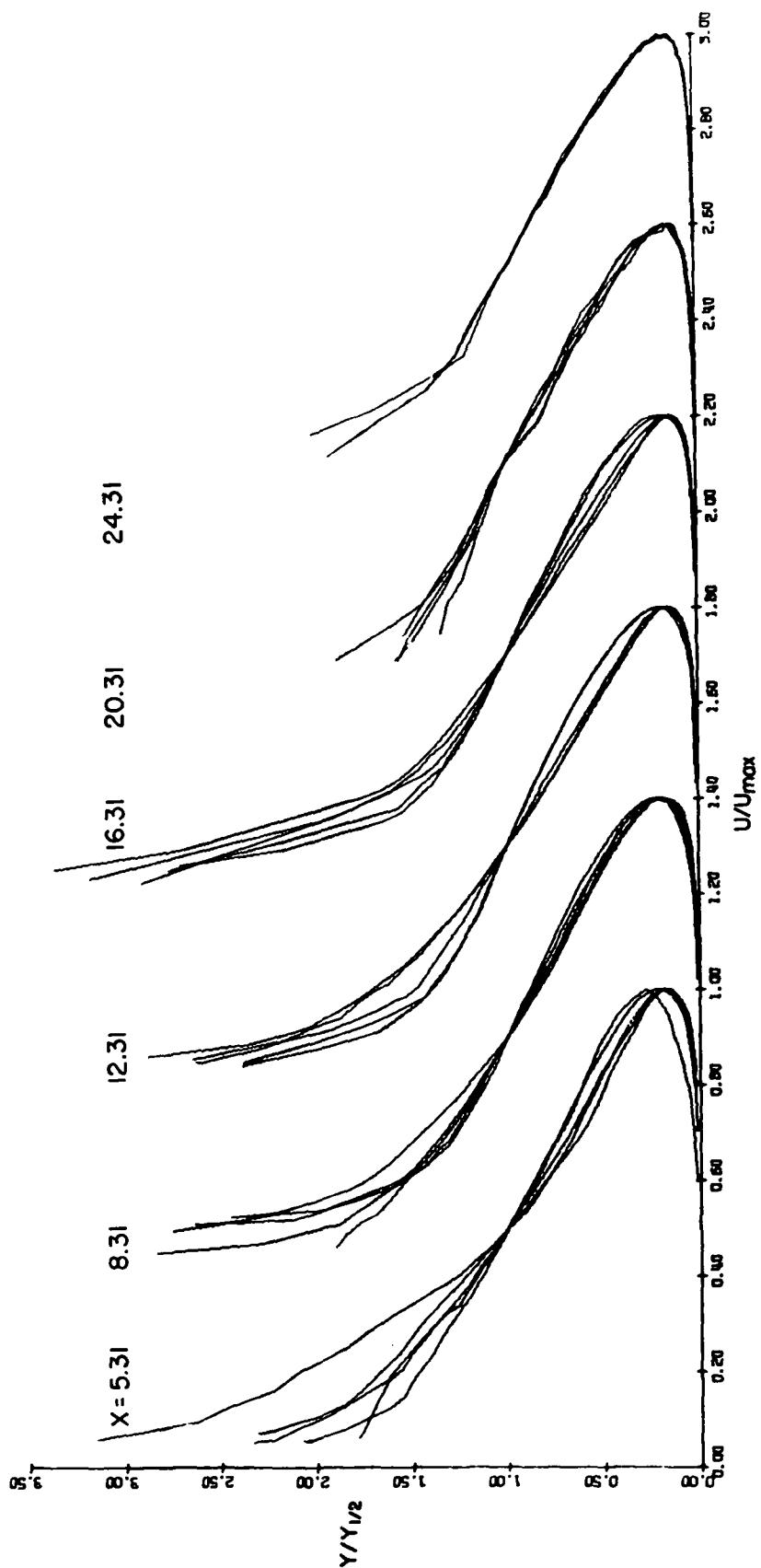
Figure 16. Multiple wall jet velocity profiles, including profiles off the centerline.

36
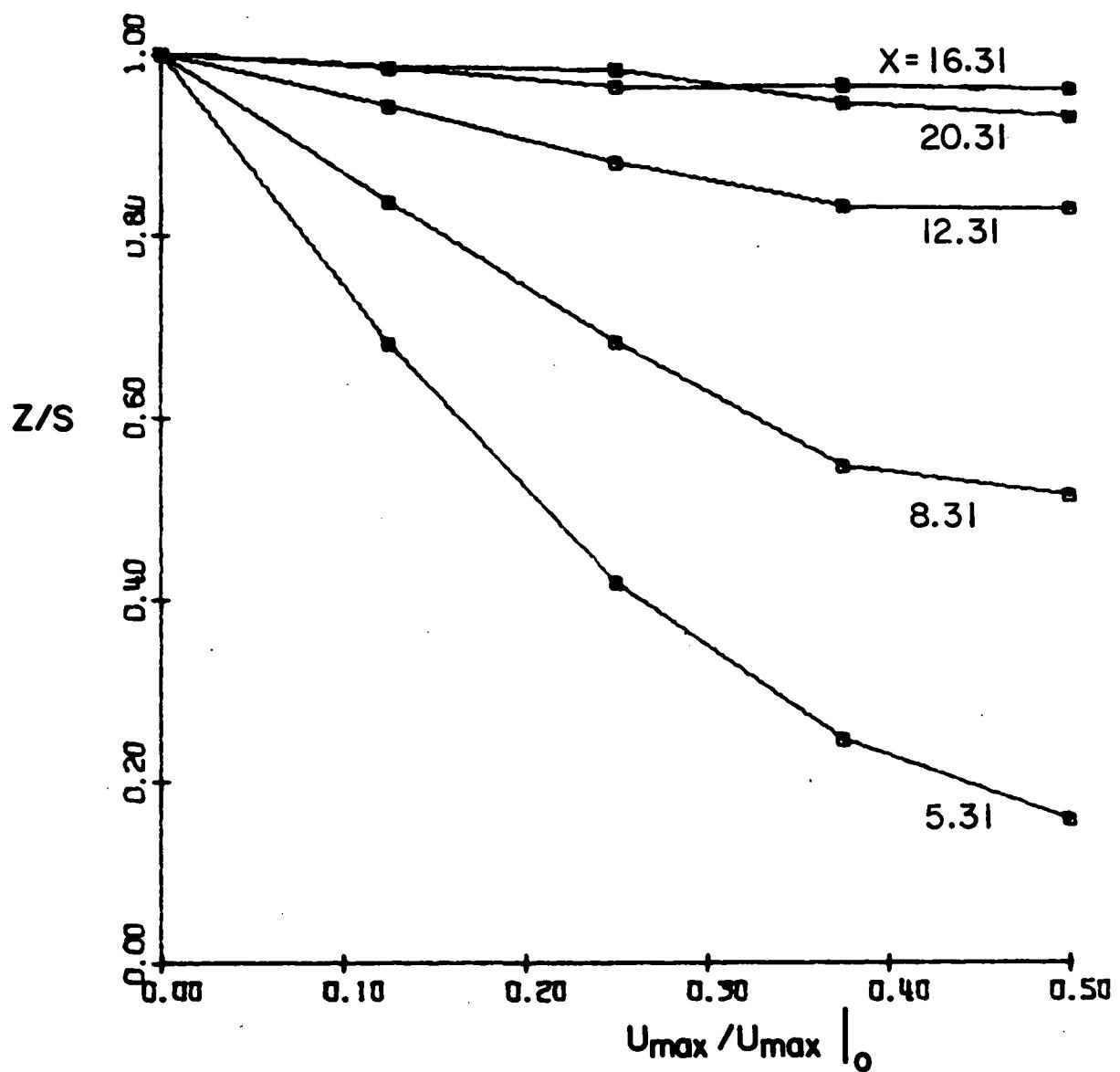
Figure 17. Transverse profiles of the maximum velocity in the multiple wall jet.

37
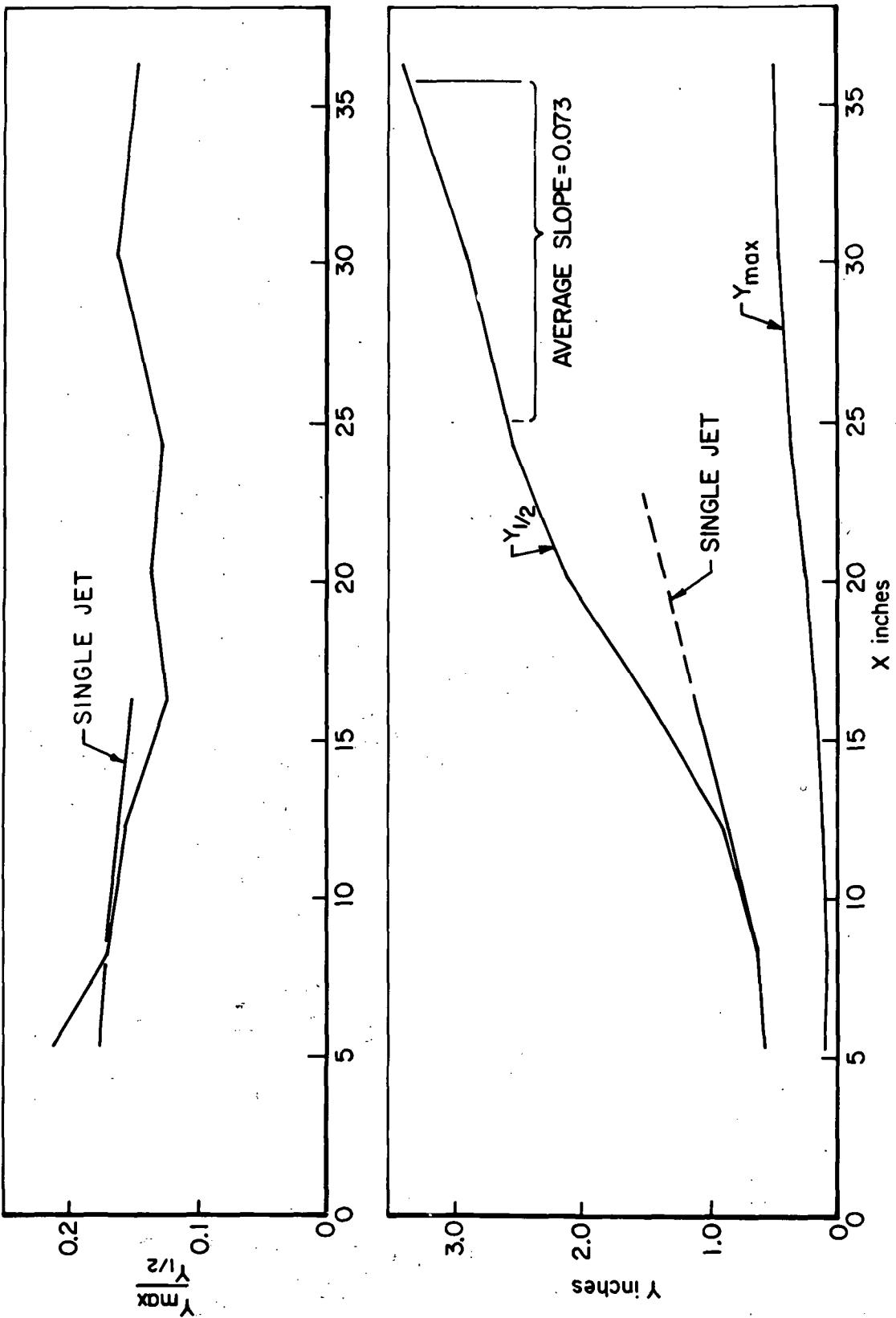
Figure 18. Axial variation of the primary length scales on a nozzle centerline of the multiple wall jet.

38
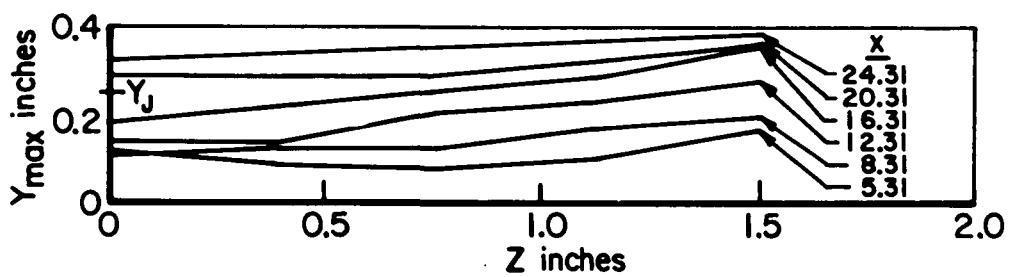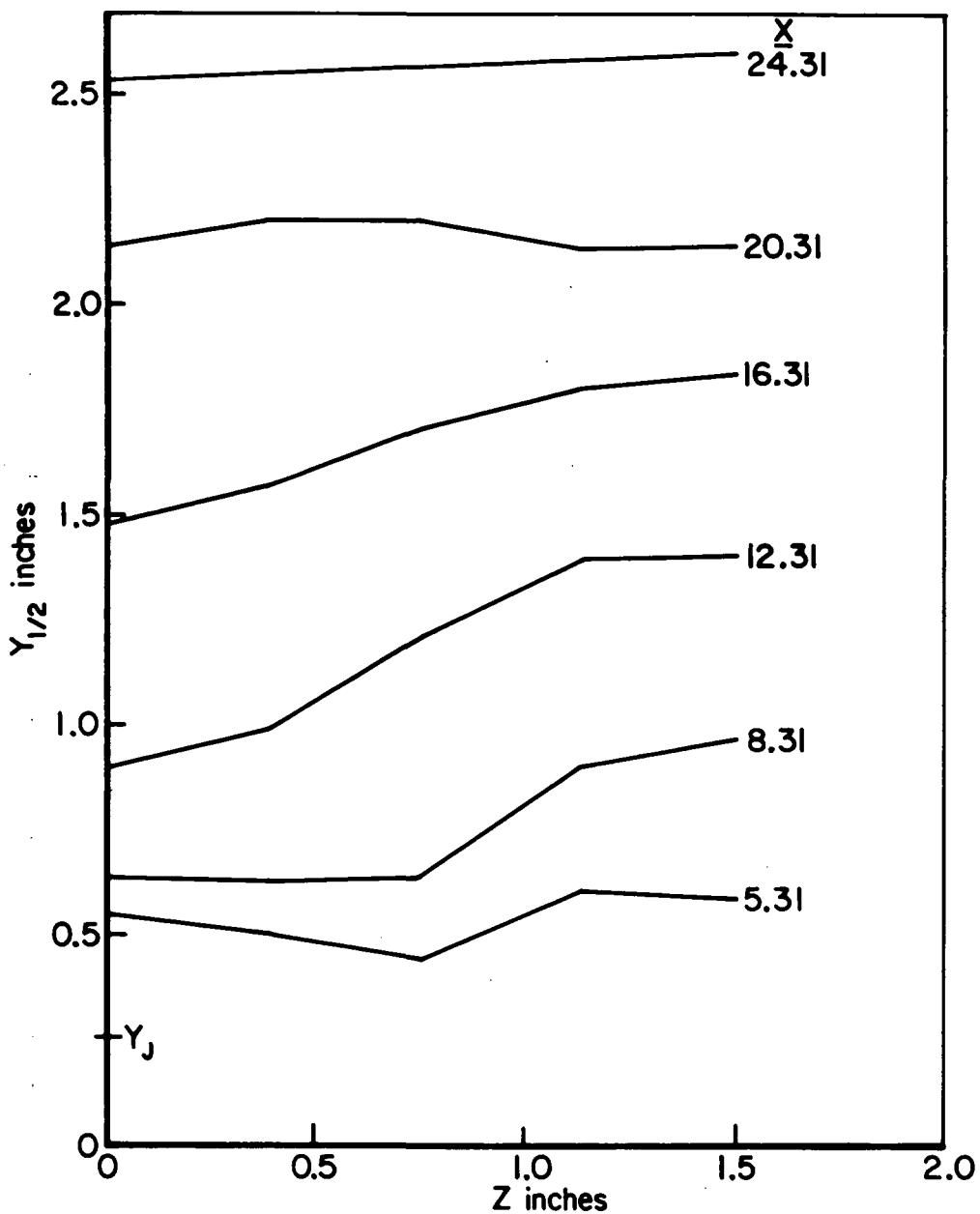
Figure 19.   Transverse variation of length scales in the multiple wall
   jet.
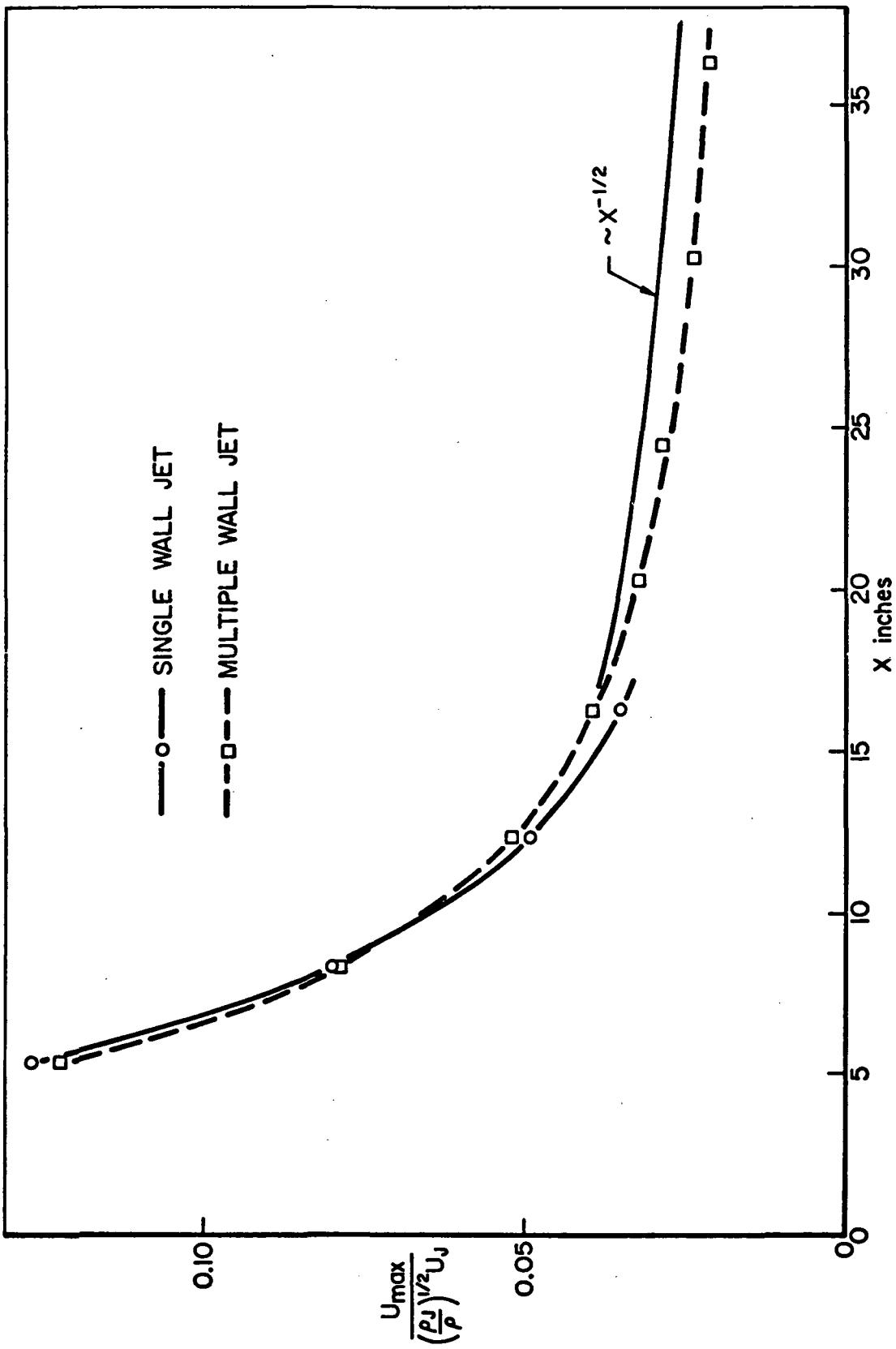
Figure 20. Axial decay of the centerline maximum velocity in the multiple wall jet.

40
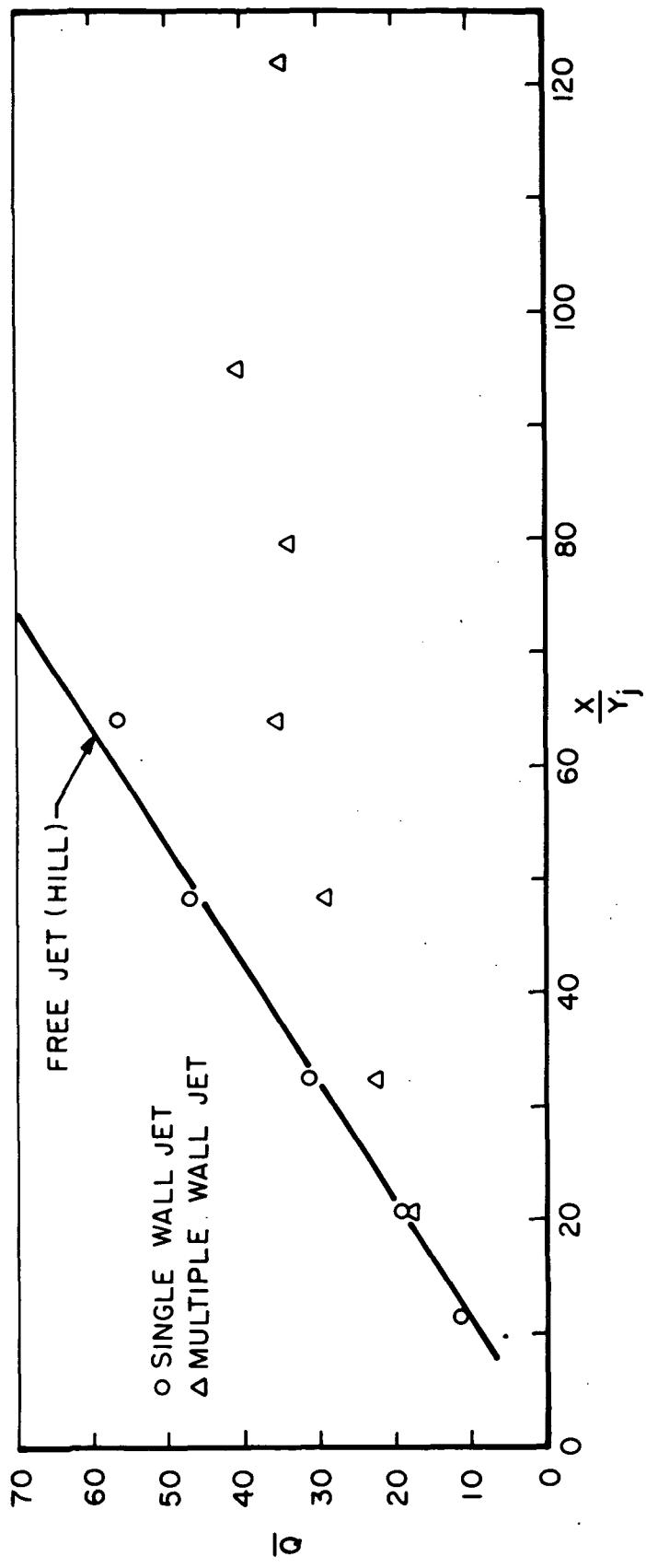
Figure 21. Integrated mass flux of the single wall jet and the multiple wall jet.
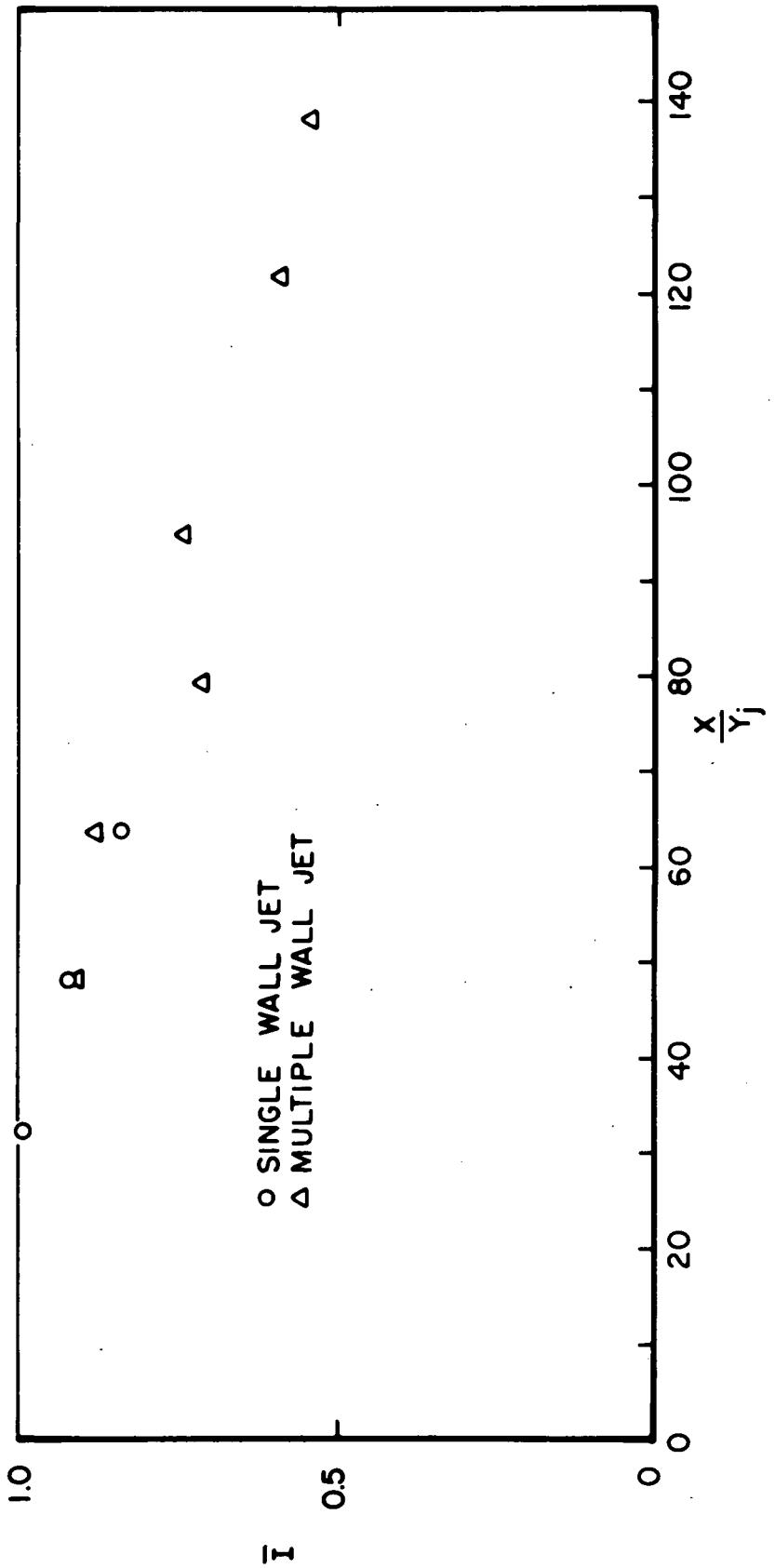
Figure 22. Integrated impulse of the single wall jet and multiple wall jet.

"The aeronautical and space activities of the United States shall be conducted so as to contribute . . . to the expansion of human knowledge of phenomena in the atmosphere and space. The Administration shall provide for the widest practicable and appropriate dissemination of information concerning its activities and the results thereof."
—NATIONAL AERONAUTICS AND SPACE ACT OF 1958

NASA SCIENTIFIC AND TECHNICAL PUBLICATIONS

TECHNICAL REPORTS: Scientific and technical information considered important, complete, and a lasting contribution to existing knowledge.

TECHNICAL NOTES: Information less broad in scope but nevertheless of importance as a contribution to existing knowledge.

TECHNICAL MEMORANDUMS: Information receiving limited distribution because of preliminary data, security classification, or other reasons. Also includes conference proceedings with either limited or unlimited distribution.

CONTRACTOR REPORTS: Scientific and technical information generated under a NASA contract or grant and considered an important contribution to existing knowledge.

TECHNICAL TRANSLATIONS: Information published in a foreign language considered to merit NASA distribution in English.

SPECIAL PUBLICATIONS: Information derived from or of value to NASA activities. Publications include final reports of major projects, monographs, data compilations, handbooks, sourcebooks, and special bibliographies.

TECHNOLOGY UTILIZATION PUBLICATIONS: Information on technology used by NASA that may be of particular interest in commercial and other non-aerospace applications. Publications include Tech Briefs, Technology Utilization Reports and Technology Surveys.

Details on the availability of these publications may be obtained from:

SCIENTIFIC AND TECHNICAL INFORMATION OFFICE

NATIONAL AERONAUTICS AND SPACE ADMINISTRATION

Washington, D.C. 20546